Methylerythritol Phosphate Pathway of Isoprenoid Biosynthesis

Lishan Zhao,[1] Wei-chen Chang,[2] Youli Xiao,[3] Hung-wen Liu,[2] and Pinghua Liu[3]

[1]Amyris, Inc., Emeryville, California 94608; email: zhao@amyris.com

[2]Division of Medicinal Chemistry, College of Pharmacy, and Department of Chemistry and Biochemistry, University of Texas at Austin, Austin, Texas 78712; email: wcchang1980@utexas.edu, h.w.liu@mail.utexas.edu

[3]Department of Chemistry, Boston University, Boston, Massachusetts 02215; email: ylxiao@bu.edu, pinghua@bu.edu

Annu. Rev. Biochem. 2013. 82:497–530

The *Annual Review of Biochemistry* is online at biochem.annualreviews.org

This article's doi: 10.1146/annurev-biochem-052010-100934

Keywords

isoprenoids, biosynthesis, enzyme mechanism, metabolic engineering, synthetic biology, methylerythritol phosphate pathway, mevalonic acid pathway, MVA, MEP

Abstract

Isoprenoids are a class of natural products with more than 55,000 members. All isoprenoids are constructed from two precursors, isopentenyl diphosphate and its isomer dimethylallyl diphosphate. Two of the most important discoveries in isoprenoid biosynthetic studies in recent years are the elucidation of a second isoprenoid biosynthetic pathway [the methylerythritol phosphate (MEP) pathway] and a modified mevalonic acid (MVA) pathway. In this review, we summarize mechanistic insights on the MEP pathway enzymes. Because many isoprenoids have important biological activities, the need to produce them in sufficient quantities for downstream research efforts or commercial application is apparent. Recent advances in both MVA and MEP pathway–based synthetic biology are also illustrated by reviewing the landmark work of artemisinic acid and taxadien-5α-ol production through microbial fermentations.

Contents

INTRODUCTION

In the literature, isoprenoid, terpenoid, and terpene are used interchangeably to refer to a class of natural products built from two isoprene units, isopentenyl diphosphate (IPP; **1**) (**Figure 1**) and dimethylallyl diphosphate (DMAPP; **2**). As one of the largest and most structurally diverse groups of natural products with more than 55,000 members (1), isoprenoids play key metabolic, structural, and regulatory roles in all kingdoms of life. In addition, many monoterpenes, sesquiterpenes, and diterpenes produced as secondary metabolites are pheromones or defensive agents and are involved in many aspects of our lives, including medicine (2, 3), flavor and fragrances (4), and nutrition (5). For decades, the mevalonic acid (MVA; **6**) pathway was thought to be the only IPP and DMAPP biosynthetic pathway (6, 7). However, the incompatibility of many isotopic labeling results with the MVA paradigm was puzzling. Efforts to resolve such discrepancies eventually led to the discovery of the 2-*C*-methyl-D-erythritol 4-phosphate (MEP; **13**) pathway, also known as the 1-deoxy-D-xylulose 5-phosphate (DXP; **12**) or nonmevalonate pathway (**Figure 1*c***) (8–10). Because many human pathogens rely exclusively on the MEP pathway for the biosynthesis of their isoprenoids, many groups have pursued the study of the enzymes on this pathway with an ultimate goal of developing inhibitors as potential drugs (11–16). In addition to the therapeutic value of the MEP pathway, mechanistic investigation of the MEP pathway enzymes has also attracted significant attention as many of them catalyze unusual chemical transformations whose mechanisms remain obscure. In this review, we summarize the recent progress in our understanding of the MEP pathway, focusing on the catalytic mechanisms of the enzymes involved. Despite high demand for the chemical and biomedical applications of many isoprenoids, their production, either from natural sources or through chemical synthesis, remains challenging. Thus, exploiting the isoprenoid biosynthetic

IPP: isopentenyl diphosphate

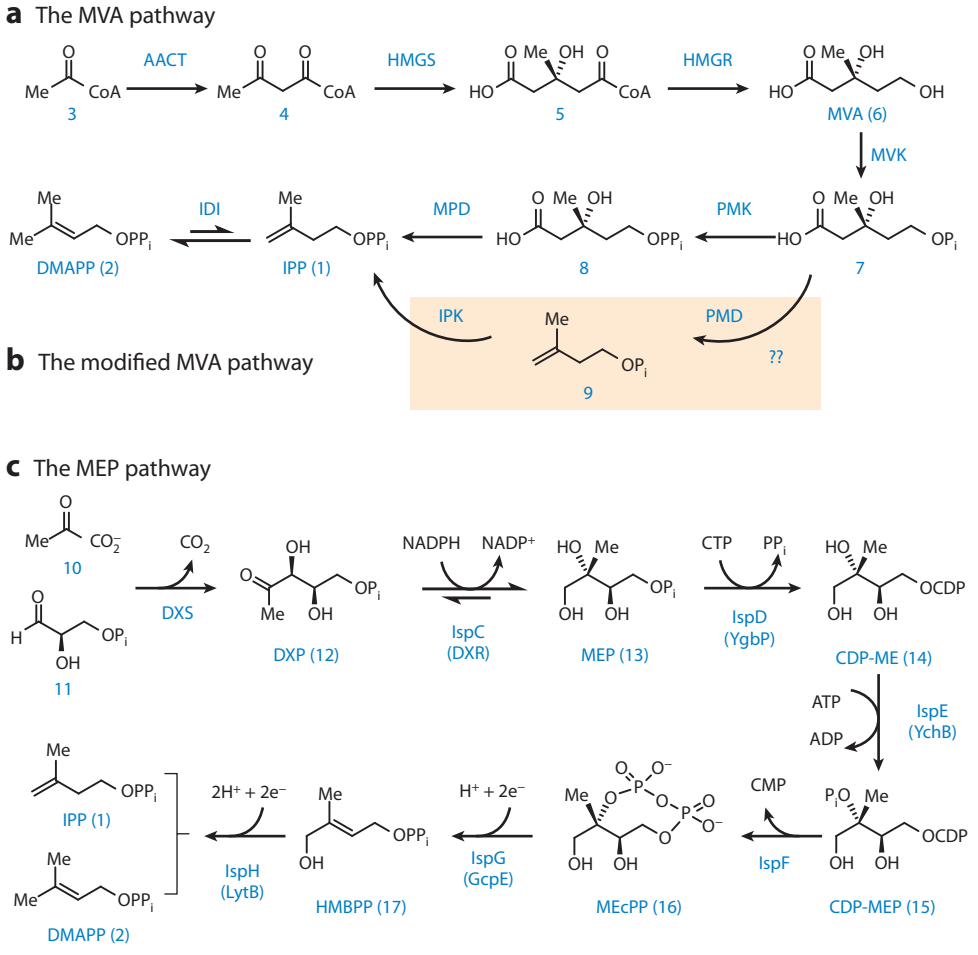

Figure 1

Pathways for the biosynthesis of isoprenoid precursors [isopentenyl diphosphate (IPP) and dimethylallyl diphosphate (DMAPP)] and their well-defined distributions among different kingdoms. (*a*) The mevalonic acid (MVA) pathway in animals, plants (cytosol), fungi, and archaea. (*b*) The modified MVA pathway in *Methanocaldococcus jannaschii*. (*c*) The methylerythritol phosphate (MEP) pathway in eubacteria, green algae, and the plastids of higher plants. Abbreviations: AACT, acetoacetyl-CoA thiolase; CDP-ME, methylerythritol cytidyl diphosphate; DXP, 1-deoxy-D-xylulose 5-phosphate; DXR, DXP reductoisomerase; DXS, DXP synthase; HMBPP, 4-hydroxy-3-methyl-butenyl 1-diphosphate; HMGR, 3-hydroxy-3-methyl-glutaryl-CoA reductase; HMGS, 3-hydroxy-3-methyl-glutaryl-CoA synthase; IDI, IPP:DMAPP isomerase; IPK, isopentenyl phosphate kinase; MEcPP, 2-*C*-methyl-D-erythritol-2,4-cyclodiphosphate; MPD, mevalonate-5-diphosphate decarboxylase; MVK, mevalonic acid kinase; PMD, phosphomevalonate decarboxylase; PMK, phosphomevalonate kinase.

machineries offers a promising approach for acquiring target isoprenoids and creating analogs not easily obtainable by synthetic means. This review also highlights some recent achievements in microbial-based isoprenoid production.

DMAPP: dimethylallyl diphosphate

MVA: mevalonate; mevalonic acid

MEP: 2-*C*-methyl-D-erythritol 4-phosphate; also known as methylerythritol phosphate

DXP: 1-deoxy-D-xylulose 5-phosphate

HMG-CoA: 3-hydroxy-3-methyl-glutaryl-CoA

HMGR: 3-hydroxy-3-methyl-glutaryl-CoA reductase

IDI: IPP:DMAPP isomerase

DXR/IspC: DXP reductoisomerase

MEcPP: 2-*C*-methyl-D-erythritol-2,4-cyclodiphosphate

IspG: 2-*C*-methyl-D-erythritol-2,4-cyclodiphosphate reductase

IspH: 4-hydroxyl-3-methyl-butenyl 1-diphosphate reductase

BIOSYNTHESIS OF ISOPRENOID PRECURSORS (ISOPENTENYL DIPHOSPHATE AND DIMETHYLALLYL DIPHOSPHATE)

For decades, the MVA pathway (**Figure 1*a***) was thought to be the only pathway for the biosynthesis of IPP (**1**) and DMAPP (**2**) (6, 7). This pathway starts with the condensation of two molecules of acetyl-CoA (**3**) to form acetoacetyl-CoA (**4**). Further condensation with a third molecule of acetyl-CoA produces 3-hydroxy-3-methyl-glutaryl-CoA (HMG-CoA; **5**), which is then reduced by HMG-CoA reductase (HMGR) to give MVA (**6**). Following two consecutive phosphorylation steps catalyzed by mevalonic acid kinase (MVK) and phosphomevalonate kinase, the resulting mevalonate-5-diphosphate (**8**) is converted to IPP (**1**) in an ATP-coupled decarboxylation reaction catalyzed by mevalonate-5-diphosphate decarboxylase. An IPP:DMAPP isomerase (IDI) is responsible for the interconversion between IPP (**1**) and DMAPP (**2**). Recently, Grochowski et al. (17) identified an enzyme from *Methanocaldococcus jannaschii* capable of phosphorylating isopentenyl phosphate (**9**) to IPP (**1**). A modified MVA pathway was thus proposed (**Figure 1*b***), in which mevalonate-5-phosphate (**7**) is decarboxylated to **9** and then phosphorylated by isopentenyl phosphate kinase to form IPP (**1**) (18–20). However, the proposed phosphomevalonate decarboxylase (**7** → **9** conversion) has yet to be identified.

The MEP pathway (**Figure 1*c***) was discovered in the 1990s (21, 22). The history of this remarkable discovery has been covered in a few reviews (8–10). The pathway is initiated with a thiamine diphosphate (TPP)-dependent condensation between D-glyceraldehyde 3-phosphate (**11**) and pyruvate (**10**) to produce DXP (**12**), which is then reductively isomerized to MEP (**13**) by DXP reductoisomerase (DXR/IspC). Subsequent coupling between MEP (**13**) and CTP is catalyzed by CDP-ME synthetase (IspD) and produces methylerythritol cytidyl diphosphate (CDP-ME; **14**). An ATP-dependent enzyme (IspE) phosphorylates the C_2 hydroxyl group of **14**, and the resulting 4-diphosphocytidyl-2-*C*-methyl-D-erythritol-2-phosphate (CDP-MEP; **15**) is cyclized by IspF to 2-*C*-methyl-D-erythritol-2,4-cyclodiphosphate (MEcPP; **16**). IspG catalyzes the ring opening of the cyclic pyrophosphate and the C_3-reductive dehydration of MEcPP (**16**) to 4-hydroxy-3-methyl-butenyl 1-diphosphate (HMBPP; **17**). The final step of the MEP pathway is catalyzed by IspH and converts HMBPP (**17**) to both IPP (**1**) and DMAPP (**2**). Thus, unlike the MVA pathway, IDI is not essential in many MEP pathway–utilizing organisms.

Clearly, the MVA and MEP pathways represent two different strategies employed by nature to synthesize the five-carbon isoprene units. In addition, there is a well-defined distribution of the MVA and MEP pathways among different kingdoms (8). The MEP pathway has been identified in eubacteria, green algae, and higher plants, whereas the MVA pathway is found in animals, plants (cytosol), fungi, and archaea. Plants are unique in that they have both MEP and MVA pathways, albeit with a compartmental segregation between them. Investigators thus proposed that the MEP pathway enzymes could be excellent targets for developing new broad-spectrum antibiotics and herbicides. This subject has been extensively discussed in many excellent recent reviews (11–16). In the following section, we summarize mechanistic studies on the MEP pathway enzymes, especially the transformations catalyzed by IspG (**16** → **17**) and IspH (**17** → **1/2**), which are mechanistically intriguing.

MECHANISTIC STUDIES OF THE METHYLERYTHRITOL PHOSPHATE PATHWAY ENZYMES

1-Deoxy-D-Xylulose 5-Phosphate Synthase

DXP synthase (DXS) is a TPP-dependent enzyme that exhibits weak sequence homology (~20% identity) to transketolase and the E1 subunit of pyruvate dehydrogenase (23, 24). It is a homodimeric protein (25) that catalyzes the condensation between pyruvate (**10**) and D-glyceraldehyde 3-phosphate (**11**) to generate DXP (**12**), which is also a precursor for vitamins B_1 (26) and B_6 (27). The DXS-catalyzed reaction, as depicted in **Figure 2*a***, starts with TPP cofactor activation. Coupling of the resulting ylide (**18**) with pyruvate (**10**) followed by decarboxylation affords a carbanion/enamine intermediate (**19**). Subsequent nucleophilic attack of the second substrate (**11**) by intermediate **19**, followed by the elimination of DXP (**12**), completes the catalytic cycle. Kinetically, the DXS-catalyzed reaction follows a sequential mechanism with pyruvate (**10**) as the first substrate (28). In the absence of **11**, DXS can catalyze the condensation between two molecules of pyruvate (**10**) to produce acetolactate.

1-Deoxy-D-Xylulose 5-Phosphate Reductoisomerase

DXR catalyzes a reversible intramolecular rearrangement reaction between DXP (**12**) and MEP (**13**), with the equilibrium favoring MEP (**Figure 1*c***) (29). Both NADPH and a divalent cation are required for catalysis (30, 31). DXR has been extensively studied as a promising target for new antimicrobial therapies (15). Current biochemical data suggest that DXR catalysis might follow a retroaldol/aldol mechanistic model (**Figure 2*b***) (30). In this model, DXP first fragments in a retroaldol manner between C_3-C_4 to generate a three-carbon (hydroxyacetone; **21**) and a two-carbon phosphate intermediate (**22**), which are then reunited by C-C bond formation through an aldol reaction to form methylerythrose-5-phosphate (**20**). NADPH reduces **20** stereospecifically to produce MEP (**13**). The **20** → **13** conversion by NADPH reduction was ruled out as the rate-limiting step in a pre–steady state kinetic isotope effect study, suggesting that one of the steps leading to intermediate **20** (**Figure 2*b***) might be rate limiting (32). Results from kinetic isotopic studies using both [3-^{2}H]-DXP and [4-^{2}H]-DXP supported such a hypothesis. For the retroaldol/aldol model, both C_3 and C_4 undergo sp^3 to sp^2 rehybridization in the fragmentation step. Therefore, both [3-^{2}H]-DXP and [4-^{2}H]-DXP should display secondary kinetic isotopic effects if the DXP fragmentation is part of the rate-limiting step. Results from studies using [3-^{2}H]-DXP and [4-^{2}H]-DXP showed normal secondary kinetic isotopic effects (1.04 ± 0.02 and 1.11 ± 0.02) and are consistent with the retroaldol/aldol mechanism (33, 34). Although the natural substrate for DXR is (3*S*, 4*R*)-DXP (**12**), the enzyme can also catalyze the production of (3*S*, 4*S*)-DXP (**23**) from (3*S*, 4*R*)-DXP (**12**) in the absence of divalent cation and NADPH. However, this reaction occurs at a rate that is orders of magnitude slower than the normal catalytic turnover rate (33). The formation of **23** was also observed in one of the reported crystal structures (35). These results were interpreted as additional lines of evidence supporting the retroaldol/aldol model, whereas another study suggests that the formation of **23** is due to spontaneous isomerization of **12** even in the absence of DXR (36). The DXR-catalyzed reaction has been explored using various substrate analogs (32, 37–40), and results from these studies are also consistent with the retroaldol/aldol condensation model.

Formation of MEcPP from the Methylerythritol Phosphate Pathway by IspD-, IspE-, and IspF-Catalyzed Reactions

IspD, IspE, and IspF catalyze the activation of MEP (**13**) and the subsequent cyclization to form MEcPP (**16**) (**Figure 1*c***). Recent reviews have discussed in detail structural studies,

DXS: DXP synthase

NADPH: nicotinamide adenine dinucleotide phosphate

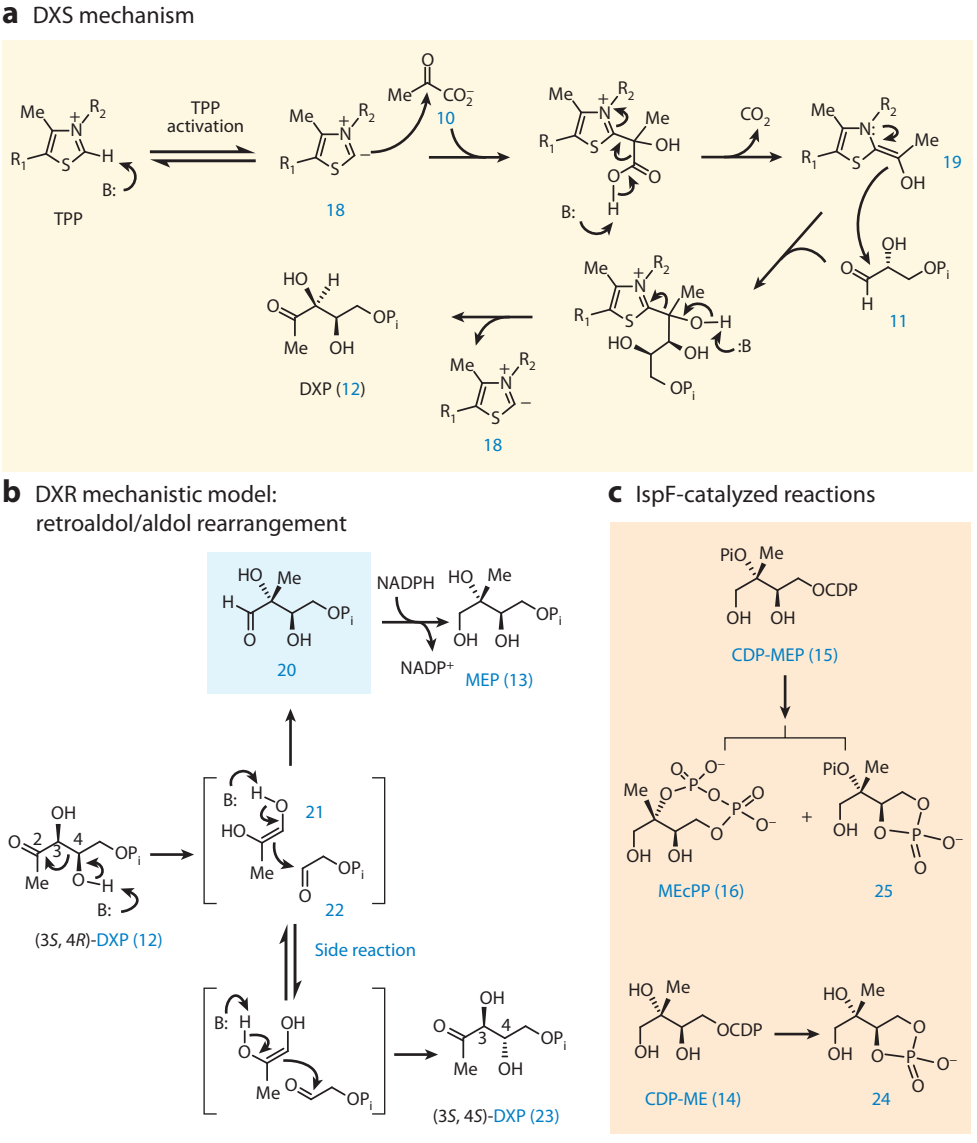

Figure 2

(*a*) Mechanism of thiamine diphosphate (TPP)-mediated condensation between pyruvate (**10**) and D-glyceraldehyde 3-phosphate (**11**) in DXS [1-deoxy-D-xylulose 5-phosphate (DXP) synthase] catalysis. (*b*) The DXR (DXP reductoisomerase) retroaldol/aldol rearrangement mechanistic model. In the retroaldol/aldol model, a side reaction may occur through the C-C bond rotation in fragment **22** followed by recombination between **21** and **22** to produce (3*S*, 4*S*)-DXP (**23**), a stereoisomer of the DXR native substrate (3*S*, 4*R*)-DXP (**12**). (*c*) Unique IspF chemistries. Besides the native IspF catalysis (**15** → **16** conversion), two more types of IspF chemistries (**14** → **24** and **15** → **25** conversions) have been discovered in some organisms. Abbreviations: CDP-ME, methylerythritol cytidyl diphosphate; CDP-MEP, 4-diphosphocytidyl-2-*C*-methyl-D-erythritol-2-phosphate; MEcPP, 2-*C*-methyl-D-erythritol-2,4-cyclodiphosphate.

biochemical characterizations, and inhibitor development of these three enzymes (14, 15). Only some unique features of these enzymes are summarized here. Besides catalyzing the physiological reaction (**15** →**16**), *Escherichia coli* and *Plasmodium falciparum* IspF can also catalyze the conversion of CDP-ME (**14**) to 2*C*-methyl-D-erythritol 3,4-cyclophosphate (**24**) (**Figure 2*c***) (41, 42). However, the rate of this reaction is only ~1% of the physiological reaction (**15** →**16**). The malaria recombinant IspF also catalyzes the formation of 2-phospho-2*C*-methyl-D-erythritol 3,4-cyclophosphate (**25**) from CDP-MEP (**15**) with a rate that is ~10% of the **15** → **16** conversion (42). Interestingly, IspDF bifunctional proteins have been found in many organisms (43–45). This type of fusion is unique in that the parent monofunctional enzymes (IspD and IspF) catalyze two nonconsecutive steps in the MEP pathway (**Figure 1*c***).

2-*C*-Methyl-D-Erythritol-2, 4-Cyclodiphosphate Reductase (IspG)

Our knowledge of the catalysis of IspG, a reductive dehydration reaction mediated by a protein containing an iron-sulfur cluster, lags far behind our understanding of the earlier enzymes in the MEP pathway. Summarized in the following section are the results collected over the past decade, including results from (*a*) characterizations of the IspG iron-sulfur cluster, (*b*) improvements to in vitro IspG activity, and (*c*) mechanistic studies on IspG. Knowledge gained in the past decade on these three aspects paves the way for more detailed IspG mechanistic studies in the future.

Characterizing the IspG iron-sulfur cluster. IspG catalyzes the ring opening of the cyclic pyrophosphate and C_3-reductive dehydration of MEcPP (**16**) to HMBPP (**17**) (46–51). Holo-IspG (52, 53) can be obtained by coexpression with an iron-sulfur cluster maturation system (e.g., *isc* operon) (54). In vivo iron-sulfur cluster assembly might also require a specific scaffold protein, ErpA (55). In vitro, the iron-sulfur cluster can be installed by the reconstitution of apo-IspG using $FeCl_3$ and Na_2S under reducing conditions (56, 57). Mössbauer characterization of the [^{57}Fe]-reconstituted IspG indicates the presence of a $[4Fe\text{-}4S]^{2+}$ cluster with one of its iron sites coordinated by a noncysteine ligand (57). This has been confirmed by the recently reported crystal structures of *Aquifex aeolicus* (58) and *Thermus thermophilus* IspGs (**Figure 3*a***) (59). The [4Fe-4S] cluster is at the C-terminal end of IspG and is coordinated by Cys265, Cys268, Cys300, and Glu307 (*A. aeolicus* IspG). The recruitment of a Glu residue as an iron-sulfur cluster ligand is rare in iron-sulfur-containing proteins (60, 61). IspG is a homodimer, and the two subunits interact with each other in a head-to-tail fashion (**Figure 3*a***). Each subunit has two domains: the N-terminal TIM-barrel domain (residues 1–254 of *A. aeolicus* IspG) that has the proposed MEcPP binding site and the iron-sulfur cluster containing the C-terminal αβ domain (residues downstream from 259 of *A. aeolicus* IspG). Within one subunit, the proposed MEcPP binding site and the [4Fe-4S] cluster are too far from each other (~56 Å) if MEcPP does directly interact with the IspG [4Fe-4S] cluster as suggested from biochemical studies (**Figure 3*a***). The IspG active site was thus suggested to be at the subunit interface, which is formed between the N-terminal domain of one subunit and the C-terminal domain of the other subunit (**Figure 3*a***) (58, 59). Results from biochemical and spectroscopic characterizations (see Mechanistic studies of IspG, below) suggest that MEcPP interacts directly with the [4Fe-4S] cluster. The proposed MEcPP binding site is still ~20 Å away from its adjacent [4Fe-4S] cluster on the other subunit (**Figure 3*a***), which raises the possibility of an MEcPP binding–triggered conformation change to bring the proposed MEcPP binding site and the [4Fe-4S] cluster into close proximity for catalysis. To date, a crystal structure of the MEcPP-IspG complex is not yet available. The MEcPP binding site shown in **Figure 3*a*** is proposed on the basis of bioinformatic analysis and site-directed mutagenesis studies.

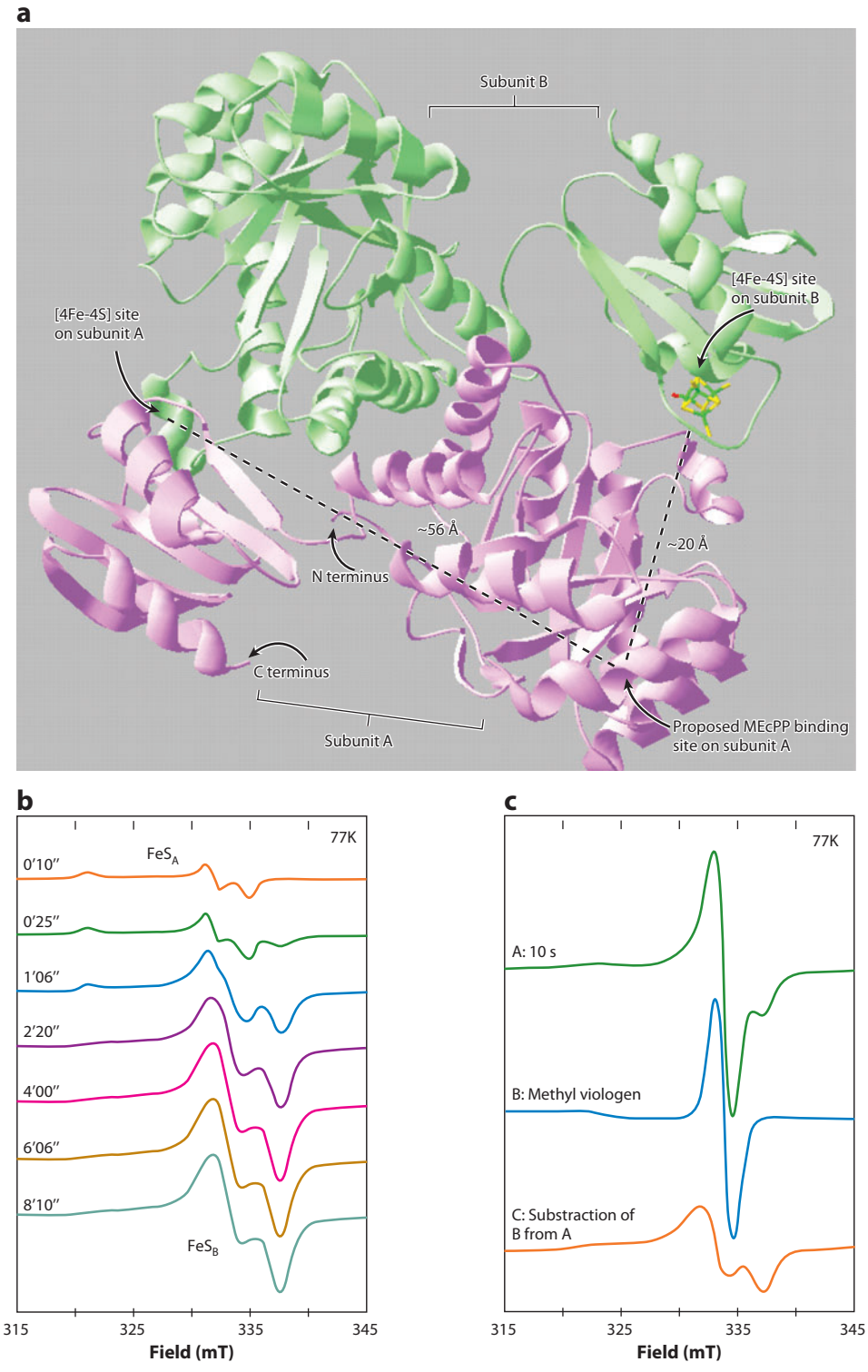

The validity of this model and the MEcPP activation mechanism remain to be established.

Improving the in vitro IspG activity. The correct installation of the IspG [4Fe-4S] cluster is essential for IspG functionality (see Characterizing the IspG iron-sulfur cluster, above). Because IspG catalysis is a reductive dehydration reaction (**Figure 1*c***), using a proper reduction system to reduce its $[4Fe\text{-}4S]^{2+}$ to a $[4Fe\text{-}4S]^{+}$ is another key factor that governs IspG activity. Puan et al. (62) proposed that flavodoxin I is the in vivo reduction system for *E. coli* IspG. Given that flavodoxins are absent in the plant plastids and the apicocomplexan plastid–like organelle, Seemann et al. (63) demonstrated that ferredoxin could support *Arabidopsis* IspG catalysis. Studies using bacterial two-hybrid system and direct pull-down assays indicated that cyanobacterial IspG also interacts with ferredoxin (64). However, results from in vitro studies suggest that other factors might also be required (53, 65). For example, when the NADPH-flavodoxin/flavodoxin reductase system was used to reduce *E. coli* IspG, there were hardly any detectable $[4Fe\text{-}4S]^{1+}$ species (<5%) based on Mössbauer and electron paramagnetic resonance (EPR) characterizations of IspG (53, 65). Systematic investigation of IspG catalysis by controlling the reduction potential of the reaction mixture using various redox dyes showed that optimal IspG activity was obtained at ~450 mV, which is ~150 mV lower than the reduction potential of the flavin cofactor in flavodoxin reductase (53). More importantly, when reduced methyl viologen was employed as the reductant ($E^0 = -446$ mV), IspG activity increased by 20-fold compared with that of the NADPH-flavodoxin/flavodoxin reductase system (53). Thus, the identity/composition of the in vivo IspG reduction system remains to be established.

The challenge of optimal reduction of the IspG iron-sulfur cluster also raises some concerns about the mechanistic relevance of the recently reported IspG paramagnetic species to IspG catalysis. When dithionite was used as the IspG reductant in steady state studies, a paramagnetic species (FeS_A, g = 2.000, 2.019, and 2.087) was observed (66). FeS_A behaves like high-potential iron-sulfur protein (HiPIP) $[4Fe\text{-}4S]^{3+}$ clusters, which have an average EPR g value greater than 2.0 and remain visible at high temperatures (e.g., 77 K). Using dithionite as the reductant, a separate study measured the time course for the formation and decay of two paramagnetic species (FeS_A and FeS_B in **Figure 3*b***) at 55°C in a thermophilic IspG. One of the two paramagnetic species was assigned as the enzyme product complex (FeS_B) (65), and the other (FeS_A) was ascribed to be the same species as the one observed in the previous steady state studies (66). For this enzyme, at 55°C, a single turnover should be complete in 2 s. However, the signals corresponding to FeS_A increased in the first 10–30 s (**Figure 3*b***). The FeS_B species maximized at 4 min and 7 s and remained discernible even at 16 min (**Figure 3*b***). In

EPR: electron paramagnetic resonance

HiPIP: high-potential iron-sulfur protein

Figure 3

X-ray crystallographic and electron paramagnetic resonance spectroscopic characterizations of IspG. (*a*) Structure of *Aquifex aeolicus* IspG. IspG is a homodimer assembled in a head-to-tail fashion. Each subunit has two domains, the proposed MEcPP-binding N-terminal domain and the C-terminal [4Fe-4S] cluster domain. The proposed IspG active site is located at the interface between the N terminus of one subunit and the C terminus of the other subunit, as the distance between the MEcPP binding site and the [4Fe-4S] cluster within the same subunit is too far for direct interactions (~56 Å). (*b*) Time course of the formation and decay of two paramagnetic species in a thermophilic IspG using dithionite as the reductant at 55°C. (*c*) Time course of the formation and decay of two paramagnetic species in a thermophilic IspG using reduced methyl viologen as the reductant. A single turnover at 25°C takes ~10 s, which is the time period of FeS_B formation (*trace C*). The FeS_A species is not observed in this scenario (*trace A*) (adapted from Reference 65).

ENDOR: electron-nuclear double resonance

contrast, when the best in vitro IspG reduction system currently available (reduced methyl viologen) was used at 25°C, FeS_A was not detected (*trace A* of **Figure 3*c***), and the FeS_B species (*trace C* of **Figure 3*c***) was observed within 10 s after the signal from methyl viologen (*trace B* of **Figure 3*c***) was subtracted from trace A of **Figure 3*c***. When reduced methyl viologen is used as the reductant at 25°C, 10 s is roughly the time period for a single turnover. Thus, the kinetic properties of FeS_A and FeS_B in **Figure 3*b*,*c***, especially the slow formation and decay of FeS_A (**Figure 3*b***), do not seem to support FeS_A as a kinetically competent intermediate leading to FeS_B formation (**Figure 3*b***) if FeS_B is indeed the IspG product complex. That only ~1–5% of the IspG iron-sulfur cluster can be reduced when dithionite is used as the direct reductant (65) is clearly a major challenge of current IspG mechanistic studies. Also, the orders-of-magnitude-lower IspG activity when using dithionite as the reductant relative to reduced methyl viologen (53, 65) is another factor that has to be considered to properly assign the catalytic relevance of these spectroscopic results. More detailed pre–steady state studies are needed to examine the kinetic compentency of these paramagnetic species.

Mechanistic studies of IspG. One of the major unresolved issues in IspG mechanistic studies is the role of the [4Fe-4S] cluster in IspG catalysis. Specifically, is it involved in substrate activation, is it the electron source, or does it have dual functions in both substrate activation and as the electron source for substrate reduction? Current IspG mechanistic models suggest that it has dual functions. The IspG crystal structure indicated that the distance between the proposed MEcPP binding site and its adjacent iron-sulfur cluster on the other IspG subunit is ~20 Å (**Figure 3*a***). If MEcPP directly interacts with the IspG iron-sulfur cluster, MEcPP binding must trigger a conformation change to bring the MEcPP binding site and the iron-cluster close in space for catalysis. In the following section, we discuss the three IspG mechanistic models and present currently available biochemical and spectroscopic evidence that supports a direct role of the iron-sulfur cluster in IspG catalysis. The structure for the paramagnetic species FeS_A in **Figure 3*b*** was also proposed whereas the kinetic competence of the FeS_A species in IspG catalysis remains an issue for the future.

Several IspG mechanistic models have been proposed over the past decade (**Figure 4**). The epoxide model proposed by Rohdich et al. (67) (**Figure 4*b***) involves 2,3-epoxy-4-hydroxy-3-methyl-butenyl 1-diphosphate (**26**) as an intermediate. This model was proposed because a synthetic [4Fe-4S] cluster can reductively deoxygenate epoxides to alkenes (68). The first step of the epoxide model is a nucleophilic attack at the C_2 position by the C_3 hydroxyl group, leading to the ring opening of the cyclic pyrophosphate and the formation of intermediate **26**. The reduced $[4Fe\text{-}4S]^+$ cluster can then mediate the reductive epoxide ring opening to form a substrate-based radical (**27**). An additional one-electron reduction generates a carbanion (**28**), which mediates the dehydration to produce HMBPP (**17**). We do not know how the substrate interacts with the iron-sulfur cluster. Coordination of the C_3-OH might facilitate the dehydration step because of the Lewis acidity of the metallocenter. The second and third models share a cation intermediate (**29**) (**Figure 4*c***), which was proposed by Seemann et al. (69) and Kollas et al. (56). In the cation model, reduction of the cation intermediate (**29**) (70) leads to a radical intermediate (**30**), which undergoes dehydration to **31** through a C-O bond cleavage mechanism as seen in radical-mediated dehydration reactions (71). Coordination of the C_3-OH group of MEcPP (**16**) to the [4Fe-4S] cluster may also facilitate the **30** → **31** transformation, as in the case of aconitase (72). Recently, a modified version of the cation model (an organometallic model) (**Figure 4*c***) was also proposed based on EPR and electron-nuclear double resonance (ENDOR) characterizations of the paramagnetic FeS_A species discussed in **Figure 3*b*** (65, 73, 74). For the organometallic model, the C_2 carbon interacts directly with

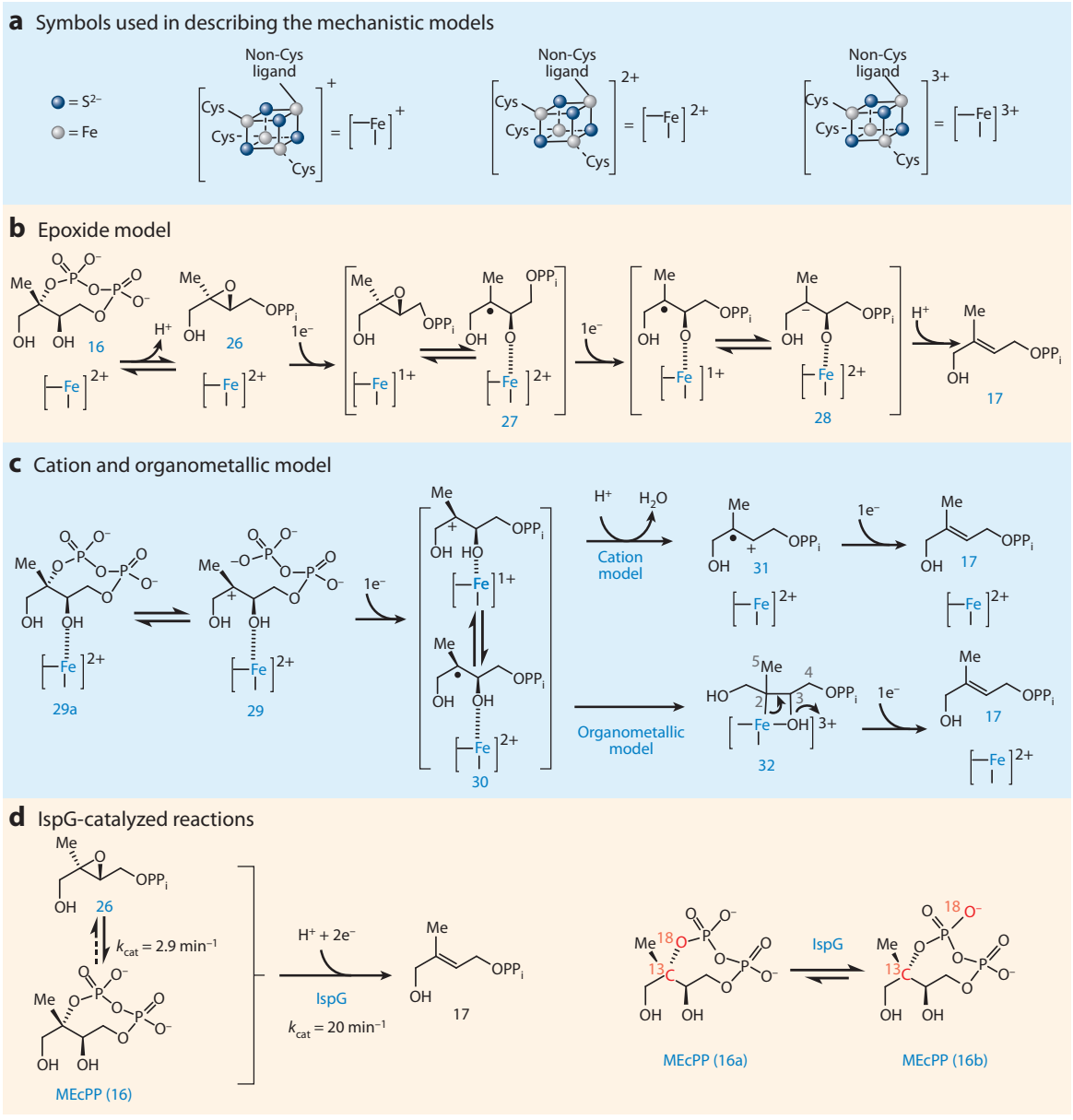

Figure 4

Proposed IspG mechanistic models. (*a*) Symbols used to represent the iron-sulfur clusters. (*b*) The epoxide model. According to this model, the epoxide (**26**) is an obligate intermediate of the MEcPP (2-*C*-methyl-D-erythritol-2,4-cyclodiphosphate) (**16**) reductive dehydration. Once the epoxide (**26**) is formed, two sequential one-electron reductions mediated by the iron-sulfur cluster lead to the formation of 4-hydroxy-3-methyl-butenyl 1-diphosphate (**17**). The Lewis acidity of the [4Fe-4S] cluster might also facilitate the dehydration process (**28** → **17** conversion). (*c*) Cation and organometallic models. In these two models, the formation of a cation intermediate (**29**) by the C_2 C-O cleavage is the first step. Once the cation intermediate (**29**) is formed, subsequent reductive dehydration can follow either the cation model via a radical cation intermediate (**31**) or the organometallic model via the organometallic intermediate (**32**). (*d*) IspG-catalyzed reactions. IspG can catalyze both the reductive deoxygenation of **26** and the reductive dehydration of **16** to **17**. However, in the absence of reductants, IspG catalyzes an irreversible **26** → **16** conversion. MEcPP (**16**) itself is stable for weeks at room temperature, whereas in the presence of holo-IspG and the absence of reductants, a positional isotope exchange (**16a** ↔ **16b**) is observed.

the [4Fe-4S] cluster unique iron site to form an Fe-C bond (**32**), and the iron-sulfur cluster is effectively a $[4Fe\text{-}4S]^{3+}$ cluster. In this model, species **32** of **Figure 4*c*** was assigned as the paramagnetic species FeS_A shown in **Figure 3*b***. Reduction of this organometallic intermediate (**32**) generates HMBPP (**17**) and regenerates the iron-sulfur cluster for the next cycle. Besides the catalytic competency issue of **32** as discussed in **Figure 3*b***, details for the **32** → **17** conversion remain to be validated, including the oxidation state of the [4Fe-4S] cluster and of the unique iron site in the proposed intermediate **32**.

IspG can utilize the epoxide (**26**) as a substrate as efficiently as it can utilize MEcPP (**16**) and produce HMBPP (**17**) as the product (**Figure 4*d***) (75). Interestingly, in the absence of reductants, IspG can irreversibly convert **26** to MEcPP (**16**) with a k_{cat} of ~2.9 min^{-1}, which is an order of magnitude slower than the steady state k_{cat} values of both the **16** → **17** and **26** → **17** conversions. Because the formation of the epoxide (**26**) has never been detected in the **16** → **17** conversion and the rate of **26** → **17** is roughly 10% of the **16** → **17** conversion (**Figure 4*d***), IspG catalysis may not involve the epoxide (**26**) as an obligate intermediate as proposed in the epoxide model (**Figure 4*b***). These kinetic studies imply that the reductive dehydration of MEcPP (**16**) and reductive deoxygenation of the epoxide (**26**) may proceed through parallel pathways (76). An important question concerning the cation model (**Figure 4*c***) is its energetic feasibility given that the C_2 position of MEcPP is unactivated (77). Such C-O bond cleavage was recently examined using the positional isotope exchange method, in which [2-^{13}C, ^{18}O]-MEcPP (**16a**) was converted to **16b** in an IspG-dependent fashion until an equilibrium was reached at the end (**Figure 4*d***). MEcPP itself is stable for weeks at room temperature, and such a positional isotope exchange depends absolutely on the presence of holo-IspG. Because the positional isotope exchange experiment was conducted in the absence of reductants, this result not only provides evidence supporting the reversible C-O bond cleavage at the MEcPP (**16**) C_2 position but also implies that the formation of a cation intermediate occurs prior to any redox chemistry (70). How IspG facilitates the MEcPP (**16**) C_2 C-O bond cleavage remains to be addressed.

The above biochemical studies are consistent with the involvement of a cation intermediate (**29**) in IspG catalysis. The downstream chemical reactions after cation formation are still controversial. After the initial report of the FeS_A species by Adedeji et al. (66), subsequent studies indicated that the same paramagnetic species (FeS_A) was observed when either the epoxide (**26**) or MEcPP (**16**) was used as the substrate (73, 74). These results can be attributed to the conversion of the epoxide (**26**) to MEcPP (**16**) (**Figure 4*d***) (76). Several additional EPR, ENDOR, and hyperfine sublevel correlation spectroscopic characterizations (65, 73, 74) of the paramagnetic species FeS_A were reported, revealing the following hyperfine tensors: [1.8, 1.6, 1.8] MHz for MEcPP C_5 deuterated methyl group and [14.5, 12.0, 26.5] MHz for the MEcPP C_2 carbon (referring to the carbon numbering system shown in the structure of species **32**) (**Figure 4*c***). Based on these parameters, Duin, Hoffman, and coworkers (65) suggested that such a paramagnetic species (FeS_A) might be either an organometallic species (**32**) (**Figure 4*c***) or the IspG-MEcPP complex (**29a**) (**Figure 4*c***). Wang et al. (73, 74) assigned it as **32**. However, because FeS_A formation and decay rates (**Figure 3*b***) do not seem to support FeS_A as a kinetically competent species, more systematic pre–steady state studies are needed in the future. Thus, the exact role of the iron-sulfur cluster and the chemistries after the formation of the cation intermediate (**29**) are not yet known.

Summary. In summary, based on Mössbauer spectroscopic and X-ray crystallographic characterizations, IspG is widely accepted as a unique iron site–containing [4Fe-4S] protein, but we do not yet know how its [4Fe-4S] cluster is involved in substrate activation and catalysis. In the past decade, a combination of

a few approaches, including the coexpression of IspG along with the *isc* operon and the use of different reduction systems, led to an improvement of IspG activity by a few orders of magnitude. However, other players might be missing as the best IspG activity is still 1–2 orders of magnitude less than that of other MEP pathway enzymes. IspG catalytic mechanisms are still highly controversial. Biochemical studies, especially the positional isotope exchange results, indicate that a cation intermediate might be feasible, whereas how IspG facilitates the cation formation remains to be addressed. Regarding the intermediates downstream of the proposed cation species (**29**), whether the reaction follows the radical cation intermediate (**31**) pathway or the organometallic intermediate (**32**) pathway is unclear (**Figure 4*c***). Several reports have emerged recently on the characterization of the paramagnetic species detected in IspG catalysis. Because of the conditions used in these studies, the activity of the enzyme is orders of magnitude less than optimal IspG activity. Thus, the kinetic competency and catalytic relevance of these paramagnetic species to IspG catalysis still need to be established by more detailed pre–steady state studies.

4-Hydroxy-3-Methyl-Butenyl 1-Diphosphate Reductase (IspH)

IspH is an iron-sulfur enzyme (78) that catalyzes the reductive dehydration of HMBPP (**17**) to IPP (**1**) and DMAPP (**2**) in a ratio of 5:1 (79). This ratio deviates significantly from the equilibrium ratio (1:3) mediated by IDI (80). Coexpression of IspH with an iron-sulfur maturation system (e.g., *isc* operon) leads to a holo-IspH with activity better than that of in vitro reconstituted IspH (81–85). As in the IspG case, when reduced methyl viologen is used as the reduction system, IspH activity can be further improved by two orders of magnitude relative to that of the NADPH-flavodoxin/flavodoxin reductase system (62, 85). Similar to IspG studies, although significant progress has been made in the past decade, many aspects of IspH catalysis are still highly controversial. IspH mechanistic studies in the past decade are summarized below in three sections: (*a*) IspH structural flexibility, (*b*) Mechanistic studies of IspH, and (*c*) Stereochemistry in IspH catalysis.

IspH structural flexibility. IspH is a [4Fe-4S] cluster–containing protein. The Mössbauer spectrum of the [^{57}Fe]-labeled IspH is consistent with the presence of a [4Fe-4S]$^{2+}$ cluster having a spin-delocalized $Fe^{2.5+}$–$Fe^{2.5+}$ pair and a spin-localized Fe^{2+}–Fe^{3+} pair (85, 86). The ferrous site of the spin-localized Fe^{2+}–Fe^{3+} pair was proposed to be the substrate binding site. This assignment is supported by the crystal structure of the IspH-HMBPP complex (**Figure 5*a***) (83) and the changes in the isomer shift and quadruple splitting in the Mössbauer spectrum that are induced by HMBPP and HMBPP analog binding (**Supplemental Figure 1** and **Supplemental Table 1**; follow the **Supplemental Materials link** from the Annual Reviews home page at **http://www.annualreviews.org**) (85–87). Over the past few years, several IspH structures (IspH alone as well as the complex with substrate, products, or substrate analogs) (**Figure 5**) have been reported. One of the important features revealed by these studies is the structural flexibility of IspH. In the following section, we discuss several different IspH conformations.

Most IspH structures determined thus far (IspH alone or in complex with IPP or DMAPP) have a [3Fe-4S]$^{+}$ cluster bound in the active site (**Figure 5*b*,*c***) (83, 88, 89). The recently resolved IspH-HMBPP complex at 1.7-Å resolution has a [4Fe-4S] cluster (**Figure 5*a***) (83), which is coordinated by three conserved Cys residues (Cys12, Cys96, and Cys197 in *E. coli* IspH), with its fourth iron coordinated by the HMBPP C_4-OH group (83). HMBPP (**17**) itself adopts a hairpin conformation sandwiched between the [4Fe-4S] cluster and its pyrophosphate group in the active site. An H-bonding network is formed through HMBPP, Thr167, Glu126, and an active site–bound water. The distance

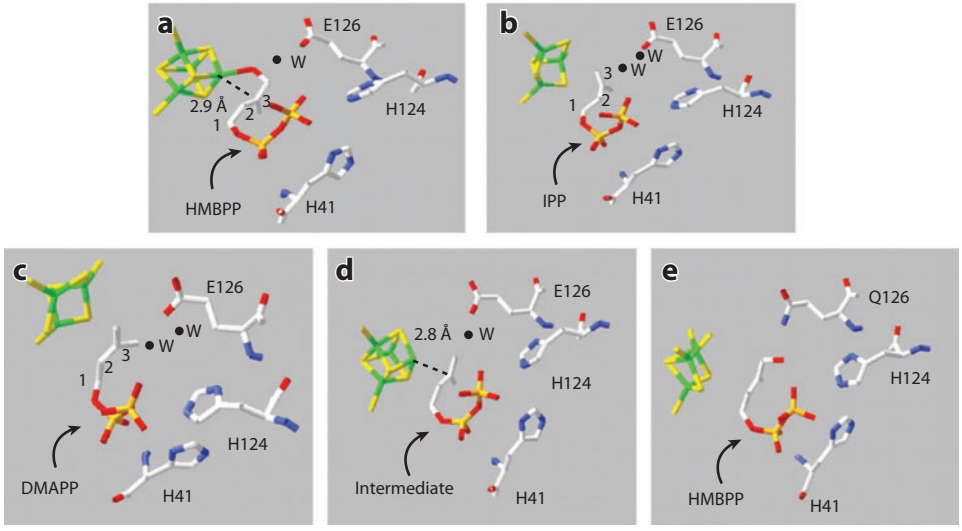

Figure 5

Representative IspH structures revealing IspH structural flexibility. (*a*) The crystal structure of the IspH-HMBPP (4-hydroxy-3-methyl-butenyl 1-diphosphate) complex at 1.7-Å resolution. This structure reveals a few important features, including the direct coordination between the HMBPP C_4-OH and the [4Fe-4S] cluster unique iron site as well as a short distance (2.8–3.0 Å) between the HMBPP olefinic functional group (C_2 and C_3 carbons) and the [4Fe-4S] cluster unique iron site. (*b*) The IspH-IPP (isopentenyl diphosphate) complex. In this structure, the active site has two water (W) molecules. In addition, the IPP C_1 carbon adopts a conformation distinct from that in the IspH-HMBPP complex in **Figure 5*a***. (*c*) The IspH-DMAPP (dimethylallyl diphosphate) complex. This structure also shows two water molecules in the active site. (*d*) On-beam conversion of the IspH-HMBPP complex. Relative to the structure in **Figure 5*a***, the HMBPP C_4-OH is gone. In addition, the distance from the HMBPP olefinic functional group (C_2 and C_3 carbons) to the [4Fe-4S] cluster unique iron site decreases to 2.6–2.8 Å. Whether this is the product complex or an intermediate is unknown. (*e*) The IspH/E126Q mutant and HMBPP complex. Relative to the structure in **Figure 5*a***, the HMBPP C_4-OH rotates to the other side of the HMBPP olefinic functional group (C_2 and C_3 carbons) and forms an internal hydrogen bond with its terminal phosphate. In this complex, there is no water in the active site and the current structure has a [3Fe-4S] cluster instead of a [4Fe-4S] cluster.

between the HMBPP olefinic carbons (C_2 and C_3) (refer to **Figure 5*a*** for the carbon numbering system) and the [4Fe-4S] cluster unique iron site is 2.8–3.0 Å, shorter than the sum of the van der Waals radii of the iron and carbon atoms (3.6 Å) but longer than the distance observed for a typical organometallic iron allylic complex (2.0–2.1 Å) (90). Thus, some interactions between the [4Fe-4S] cluster unique iron site and the HMBPP olefinic moiety are possible. In the IspH product complex (**Figure 5*b*,*c***) (83), the IPP C_1 adopts an orientation distinct from that of HMBPP (C_1-C_2 bond orientations in **Figure 5*a*** versus **5*b***). There is also an additional water molecule in the active site (**Figure 5*a*** versus **5*b***). The differences (**Figure 5*a*** versus **5*b*,*c***) in substrate/product orientations in the active site and the number of waters clearly show that the IspH active site can adopt a few different conformations.

Prolonged exposure of the IspH-HMBPP complex to X-ray irradiation results in two changes: (*a*) the distance from C_2 and C_3 of HMBPP to the [4Fe-4S] cluster unique iron site reduces to 2.6–2.8 Å, and (*b*) the electron density of the C_4 alkoxide group vanishes (**Figure 5*d***). Such changes are attributed to reductive dehydration of HMBPP, likely triggered by the solvated electrons created by the

X-ray photons. The water product from the reductive dehydration may be disordered because no extra water molecule was noted. Interestingly, in the IspH/E126Q-HMBPP complex (**Figure 5*e***), the HMBPP C_4-OH does not coordinate to the [4Fe-4S] cluster and instead adopts a completely different conformation; it rotates to the other side of the HMBPP double bond to form an internal H bond with its β-phosphate group (91). ENDOR spectroscopic analysis of this mutant in solution also implicates a similar structure (see next section for discussion) (92, 93). Whether this conformation (**Figure 5*e***) represents a catalytically relevant intermediate is uncertain because the IspH/E126Q mutant is orders of magnitude less active than the wild-type IspH. In addition, the iron-sulfur cluster in this structure (**Figure 5*e***) is in the [3Fe-4S] state instead of the active [4Fe-4S] state. Recently, it was suggested that such a new conformation (**Figure 5*e***) in the IspH/E126Q mutant also exists in wild-type IspH as a minor species (91).

Mechanistic studies of IspH. Several models have been proposed for IspH catalysis (67, 84, 92, 94–97) (**Figure 6**). The Birch reduction and organometallic models are the two currently viable mechanisms that are under consideration. In both models, the reaction is initiated by the coordination of HMBPP C_4-OH to the $[4Fe\text{-}4S]^{2+}$ unique iron site (**33**) (**Figure 6**). This step is supported by extensive biochemical (94, 95, 98, 99), Mössbauer (85–87), and crystallographic evidence (83, 96). In the Birch reduction model (67, 83, 85, 94–96), reduction of HMBPP (**17**) by the reduced $[4Fe\text{-}4S]^{+}$ cluster generates a radical anion intermediate (**34**) (**Figure 6*b***), the formation of which triggers C_4 dehydration to an allylic radical $[4Fe\text{-}4S]^{2+}$ intermediate (**35**). The second one-electron reduction (**35** → **36**) followed by protonation produces IPP (**1**) and DMAPP (**2**) (Route I) (**Figure 6*b***). Intermediate **35** may also exist in equilibrium with the allylic anion $[4Fe\text{-}4S]^{3+}$ (**37**), and its protonation can lead to the product $[4Fe\text{-}4S]^{3+}$ intermediate (**38**) (Route II) (**Figure 6*b***). In the organometallic model, following the initial IspH-HMBPP complex formation (**33**) (92), the HMBPP olefinic group interacts with the [4Fe-4S] cluster to form a π-complex or an η^2-alkenyl/metallacycle intermediate (**39**) (**Figure 6*c***). Formation of **39** is accompanied by the rotation of HMBPP C_4-OH to the other side of the HMBPP double bond to form an internal H bond with the β-phosphate group, as shown in **39**. Dehydration of **39** gives an η^1-allyl intermediate (**40**), which is likely in equilibrium with an allylic anion $[4Fe\text{-}4S]^{3+}$ species (**37**). Subsequent reduction and protonation yield IPP (**1**) and DMAPP (**2**). The two mechanistic models are similar in many aspects and share several common intermediates (species **33**, **36–38**). The main difference between them is the role of the [4Fe-4S] cluster in the catalysis. Besides serving as an anchor to bind the substrate, the [4Fe-4S] cluster in the Birch reduction model carries out reductive dehydration in a stepwise one-electron/one-electron transfer manner. It also functions as a Lewis acid to directly assist the C-O bond cleavage at C_4. The involvement of substrate-based radical intermediates (**34** and **35**) is specific to the Birch reduction model. In the organometallic model, besides a metallacycle formation–triggered (**39**) ligand replacement and bond rotation, the other important feature is the iron-sulfur cluster–mediated two-electron chemistry. According to the organometallic model, the reductive C-O bond cleavage step (**39** → **40**) is a type of two-electron chemistry and the iron-sulfur cluster is oxidized from a $[4Fe\text{-}4S]^{+}$ to a $[4Fe\text{-}4S]^{3+}$ state. Mössbauer studies have indicated that the IspH [4Fe-4S] cluster unique iron is spin localized and is at the +2 state (85–87). Thus, the change in oxidation state for the [4Fe-4S] cluster unique iron in the reductive C-O bond cleavage step (**39** → **40**) also needs to be addressed in the future if this model is followed.

Results from many biochemical studies are consistent with the Birch reduction model. To assess the energetic contributions of various interactions in the active site during IspH catalysis and to gain insight into the catalytic

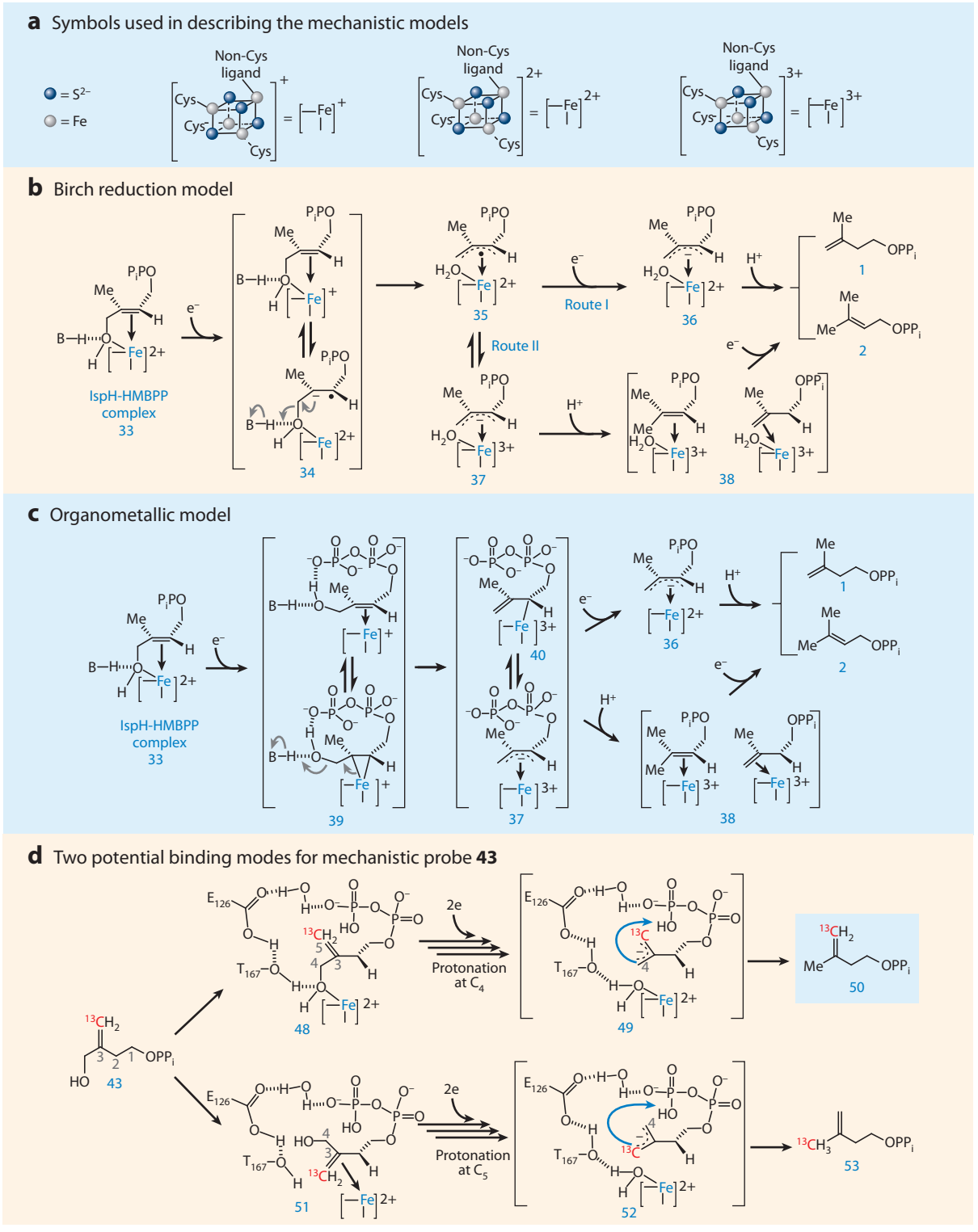

mechanism of IspH, a series of substrate analogs was prepared as probes (**41–47**) (**Table 1**) (98, 99a). The [4-F] analog (**41**), which has a fluoro substituent at C_4, can be processed by IspH to produce IPP and DMAPP in a ratio of 7:1 (95). The ~115-fold reduction in k_{cat}/K_m may result from the substitution of the C_4-OH by a fluorine atom, which reduces the proposed interaction between the substrate and the [4Fe-4S] cluster, as alkyl fluoride is a poor metal ligand. Similar results were also noted with compound **42**, which has a fluoro group at C_5 instead of C_4 and can be converted by IspH to IPP (**1**) as the sole product. The significant reduction in k_{cat}/K_m for **42** relative to HMBPP (~1,783-fold reduced) is attributed to changes in the hydrogen-bonding network with the active site residues T167 and E126, in addition to the lack of direct coordination of **42** to the [4Fe-4S] cluster (**Figure 5*a***). The structure of the IspH and substrate analog **41** complex was reported very recently. Interestingly, analog **41** adopts a conformation different from those structures discussed in both **Figure 5*a*** and **Figure 5*e*** (100). Reasons for the dramatic reduction in catalytic efficiency for mechanistic probe **42** relative to **41** will need to be further explored in the future, and the changes in coordination and H-bonding network could be the key reasons (**Table 1**). In addition, the fact that IspH can also utilize the pyrophosphonate analog (**44**) as a substrate rules out the possibility of a C-O bond scission at the C_1 position as part of the IspH catalysis (95).

More recently, [5-^{13}C]-3-(hydroxymethyl) but-3-en-1-yl diphosphate (**43**) (**Table 1**) was designed to probe whether **43** shows any preference toward the two possible coordination modes (**48** versus **51** in **Figure 6*d***) to the $[4Fe\text{-}4S]^{2+}$ cluster (98). If the C_4-OH of **43** is the anchor (**48** in **Figure 6*d***), protonation mediated by pyrophosphate at C_4 of the allylic anion intermediate (**49**) would give [^{13}C]-IPP (**50**) as the product. In contrast, if the reaction proceeds via an η^2-alkenyl intermediate (**51** in **Figure 6*c***), protonation of the allylic anion at the carbon closer to pyrophosphate (now C_5) (**52**) should yield [^{13}C]-IPP (**53**). The observation that **50** is the sole product after incubation strongly suggests that the C_4-OH group plays the dominant role in orienting the substrate. Indeed, X-ray crystallography confirmed that **43** binds to IspH using its hydroxyl group as the ligand (93). Although many pieces of biochemical evidence are consistent with the Birch reduction model, none of the key intermediates (**34–38**) (**Figure 6*b***) has been trapped and characterized. In addition, based on the feeding studies using isotopically labeled precursors, it was suggested very recently that IspH catalysis involves a C_3-C_4 bond rotation (102). Once this result is confirmed by future biochemical studies, the Birch reduction model will have to be revised to incorporate this feature if IspH catalysis indeed follows a stepwise one-electron chemistry (**Figure 6*b***) instead of a one-step two-electron chemistry (**Figure 6*c***).

The organometallic model has been proposed mainly on the basis of EPR characterization of some paramagnetic species. The IspH $[4Fe\text{-}4S]^{2+}$ cluster can be reduced by dithionite to a $[4Fe\text{-}4S]^{+}$ cluster (78, 92). When IspH E126A or E126Q mutants are reduced by dithionite, a paramagnetic species with *g* values of 2.124, 1.999, and 1.958 is observed

Figure 6

Proposed IspH mechanistic models. The formation of the IspH-HMBPP (4-hydroxy-3-methyl-butenyl 1-diphosphate) complex (**33**) is the only well-established step, and steps after **33** are highly debated (Birch reduction model versus organometallic model). (*a*) Symbols used to represent the iron-sulfur clusters. (*b*) Birch reduction model. In this model, the IspH iron-sulfur cluster has two roles: mediating two stepwise one-electron reduction steps (**33** → **34** and **35** → **36**) and serving as the Lewis acid to facilitate C_4 dehydration (**34** → **35**). (*c*) Organometallic model. In this model, there are also two unique features: the rotation of the HMBPP C_4-OH group away from the [4Fe-4S] cluster to form an internal H bond (**39**) and an iron-sulfur cluster–mediated one-step two-electron reduction (**39** → **40**). (*d*) Two possible binding modes for mechanistic probe **43** (**48** versus **51**).

Table 1 Various mechanistic probes used to study IspH catalysis

Probes	Compound number	k_{cat} (min^{-1})	K_m (μM)	k_{cat}/K_m (μM^{-1} min^{-1})	Product	Product ratio
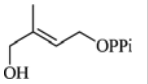	17	604 ± 17	19.7 ± 2.4	30.6	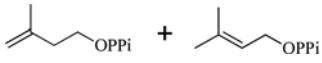	IPP:DMAPP ~ 5:1
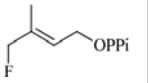	41	27.7 ± 2.2	104 ± 31	0.27	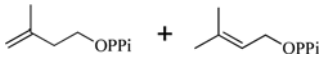	IPP:DMAPP ~ 7:1
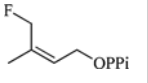	42	8.4 ± 1.9	489 ± 170	0.02	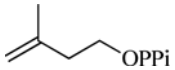	Only IPP
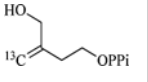	43	484 ± 1.5	694± 74	0.68	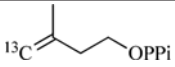	Only IPP
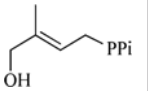	44	0.55	3950	[a]2.52×10^{-4}	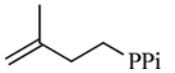	Only IPP analog
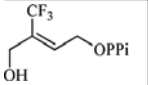	45	91.6 ± 2.2	447 ± 32	0.21	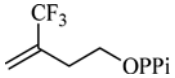	Only IPP analog
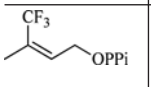	46	No detectable activity				
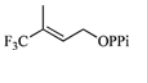	47	No detectable activity				

[a]Kinetics for this analog was determined using the NADPH-flavodoxin/flavodoxin reductase system instead of reduced methyl viologen for all of the other analogs.

Abbreviations: DMAPP, dimethylallyl diphosphate; IPP, isopentenyl diphosphate.

(92). The hyperfine parameters obtained from ENDOR characterizations of this species are consistent with the reported structure of the IspH/E126Q-HMBPP complex (**Figure 5*e***; **39** in **Figure 6*b***). Although the EPR/ENDOR data match the E126Q crystallographic results, the catalytic relevance of this paramagnetic species remains to be verified because the E126 mutants have activities orders of magnitude less than wild-type IspH. Recently, Duin, Hoffman, and coworkers (97) reported a different paramagnetic species with *g* values of 2.173, 2.013, and 1.997 using wild-type IspH. Such a paramagnetic species was observed upon mixing HMBPP with dithionite-prereduced IspH. The same paramagnetic species was also observed in steady-state studies using dithionite as the reductant by Oldfield and coworkers (93). Because the average *g* value is greater than 2.0 and the temperature dependence is more like that of a HiPIP $[4Fe\text{-}4S]^{3+}$ cluster, this paramagnetic species was proposed to be the allylic anion $[4Fe\text{-}4S]^{3+}$ intermediate (**37**) (93). To fully establish its chemical nature, one needs

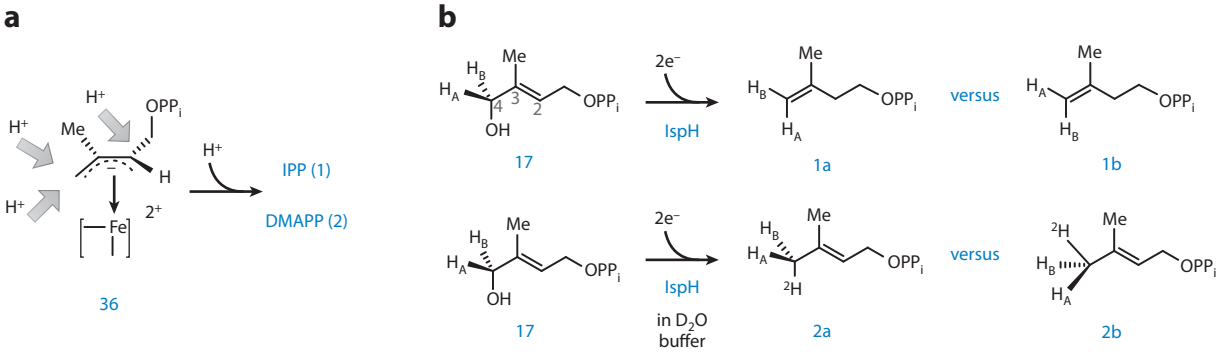

Figure 7

Stereochemistries in IspH catalysis. (*a*) The proposed allylic anion intermediate in IspH catalysis. (*b*) The DMAPP (dimethylallyl diphosphate) C_4 methyl and IPP (isopentenyl diphosphate) terminal olefinic hydrogen stereochemistries are governed by two factors, the C_3-C_4 bond rotation and the source for C_4 protonation of intermediate **36**.

to determine its oxidation state. If it is indeed a $[4Fe\text{-}4S]^{3+}$ species, the next step is to determine whether it is **37** or the $[4Fe\text{-}4S]^{3+}$ product complex (**38**), because the proton source (the pyrophosphate group) (**Figure 6*b***) is nearby and the protonation of the substrate-based anionic intermediate (**37**) should be facile. Also important is that the IspH turnover number is $>10\ s^{-1}$ under optimal conditions, and thus a single turnover should be complete in 0.1 s (85, 96). That the paramagnetic species with *g* values of 2.173, 2.013, and 1.997 was produced on a timescale of seconds to up to tens of minutes (93, 97) casts doubt on its catalytic competency. Thus, a more systematic pre–steady state kinetic analysis of these paramagnetic species is needed to demonstrate the kinetic competency of these paramagnetic species.

Stereochemistry in IspH catalysis. Following either the Birch reduction or the organometallic model, protonation of the allylic anion intermediate (**36**) is the last step (**Figure 7*a***). Examination of the structure of the IspH-HMBPP complex (**Figure 5*a***) suggests that the HMBPP pyrophosphate might serve as a potential proton source for C_2 protonation. Such a predicted *pro-S* stereospecificity at the C_2 position was biochemically confirmed recently (101). However, the IPP terminal olefinic methylene stereochemistry remains to be determined (**1a** versus **1b**) (**Figure 7*b***). In the Birch reduction model, the absence of C_3-C_4 bond rotation in **17** suggests IPP (**1a**) (**Figure 7*b***) to be the sole product. In contrast, turnover via the organometallic model gives IPP (**1b**) as the anticipated product as a result of the **33** → **39** conversion (**Figure 6*c***). Protonation at C_4 of the allylic intermediate (**36**) (**Figure 7*a***) produces DMAPP (**2a** or **2b**). Again, the DMAPP stereochemistry depends on whether the reaction involves a C_3-C_4 bond rotation step, and whether pyrophosphate or the water molecule generated from C_4-OH dehydration is the C_4 proton source (**Figure 7*a***). Recently, results of gas chromatography–mass spectrometry analysis of terpenes isolated from *Streptomyces avermitilis* fed with isotopically labeled deoxyxylulose were cited as evidence supporting the presence of C_3-C_4 bond rotation in IspH catalysis (102). Owing to the participation of IDI in the transformation, labeling results from in vivo studies are complicated (8, 9, 102–105), and more detailed in vitro biochemical studies in the future will provide further evidence for this important mechanistic issue.

Summary. In the past decade, significant progress has been made in IspH catalysis, including the improvement of IspH activity

by several orders of magnitude following the optimization of its iron-sulfur cluster maturation and reduction systems. That HMBPP coordinates to the [4Fe-4S] cluster through its C_4-OH group is well accepted (**33**) (**Figure 6**), whereas steps after the HMBPP-IspH complex formation are still highly debated (Birch reduction versus organometallic models) (**Figure 6*b*,*c***). Trapping and characterizing kinetically competent intermediates and integrating structural, kinetic, spectroscopic, and biochemical information will fill this knowledge gap.

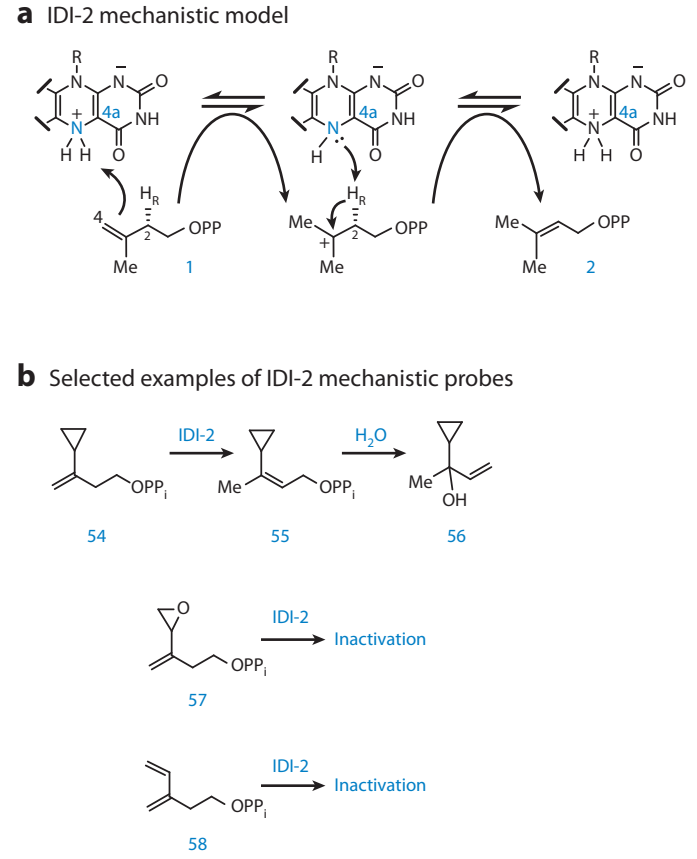

Figure 8

IDI-2 (dimethylallyl diphosphate isomerase) mechanistic model and selected mechanistic probes. (*a*) IDI-2 mechanistic model. The flavin cofactor functions as both acid and base to complete the catalytic cycle. (*b*) A few selected IDI-2 mechanistic probes to examine the IDI-2 radical versus acid/base chemistry.

Type II Isopentenyl Diphosphate: Dimethylallyl Diphosphate Isomerase (IDI-2)

IDI is responsible for the interconversion between IPP (**1**) and DMAPP (**2**). Although IDI is not essential for the MEP pathway–utilizing organisms, it functions to balance the ratio between IPP and DMAPP to meet the demands under various cellular conditions. There exist two structurally unrelated IDI enzymes, the type I isomerase (IDI-1) and the type II enzyme (IDI-2). IDI-1 was identified in the 1950s as a Zn^{2+}-dependent metalloprotein (106, 107), whereas IDI-2 was discovered in 2001 (108) and requires reduced flavin mononucleotide (FMN) and Mg^{2+} for activity (108–110). Because isomerization between IPP and DMAPP involves no net change in the redox state of the substrate/product, the exact role of the IDI-2-bound FMN in catalysis has been the focus of extensive research in recent years. Aerobically isolated IDI-II is yellow in color because of the presence of an oxidized FMN coenzyme (108), which can be readily reduced by NADPH or another reductant (e.g., dithionite). Quantitative analysis of NADPH consumption and product formation reveals that only catalytic quantities of NADPH are required to activate the enzyme, after which the reduced IDI-2 remains catalytically competent for multiple turnovers under anaerobic conditions (110, 111).

Most mechanistic studies on IDI-2 have focused on differentiating between two mechanisms, a radical model and an acid/base model. The radical model involves the transient flavin semiquinone/substrate radical pair. The acid/base model has a proton addition-elimination mechanism similar to IDI-1. Current evidence supports the mechanistic model in **Figure 8*a***, in which the flavin cofactor functions as acid and base to complete the catalytic cycle. The radical model is less likely, based on several lines of evidence. First, despite the detection of a flavin radical in an early study (110), its low concentration and the lack of a corresponding substrate-based radical argue against its catalytic relevance (111, 112).

Secondly, stopped-flow studies under single-turnover conditions also failed to detect a predicted flavin semiquinone species (112). Finally, no ring-opened or rearrangement product is produced at a detectable level when a few radical clocks (e.g., **54** in **Figure 8*b***) are used (113, 114).

Recent structural, kinetic, and biochemical studies are all consistent with reduced flavin–mediated acid/base chemistry in IDI-2 catalysis (**Figure 8*a***). X-ray crystal structures of the reduced IDI-2 in complex with either IPP or DMAPP reveal a lack of acidic/basic amino acid residues in the vicinity of the substrate (115). Instead, the substrate appears to stack closely on top of the flavin cofactor, with its C_2 atom positioned ~3 Å away from N_5 of FMN. Furthermore, the IPP *pro-R* C_2-H, which is stereoselectively removed during IDI-2 turnover (116), appears to be oriented toward the flavin cofactor N_5 atom. These observations suggest that the reduced FMN coenzyme of IDI-2 may play a direct role in mediating a protonation/deprotonation mechanism. Studies using a series of FMN analogs substituted at the 7 and 8 positions of the isoalloxazine moiety with various electron-donating and -withdrawing groups also strongly support the reduced flavin as an acid/base catalyst (117). Lastly, additional evidence supporting acid/base chemistry came from studies using IDI-2 inhibitors. When epoxide and diene analogs of IPP (**57, 58**) (**Figure 8*b***) were examined, time-dependent IDI-2 inactivation by covalent flavin modification at its C_{4a} position was observed (114, 118–120). Moreover, chiral methyl analysis of the DMAPP products derived from the IDI-2 catalyzed reaction with (*E*)- and (*Z*)-[4-^{3}H]-IPP in D_2O provides strong support for a chemical mechanism involving a flavin-mediated protonation at the vinyl C_4 position of the bound IPP substrate (121). Solvent kinetic isotope effect and proton inventory studies suggest that this proton transfer may be partially rate limiting during steady-state IDI-2 turnover (112). When taken into consideration with the body of IDI-2 biochemical, kinetic, and structural studies, these results are most consistent with a mechanism involving reduced flavin-mediated acid/base chemistry at both C_2 and C_4 of IPP/DMAPP (**Figure 8*a***).

ISOPRENOID PRODUCTION THROUGH METABOLIC ENGINEERING

As one of the most structurally diverse classes of natural products (1, 122), isoprenoids have found applications in areas of medicine [e.g., the antimalarial drug artemisinin (**64**) (2) and the anticancer drug Taxol® (**68**) (3)], flavor and fragrances [e.g., essential oils (4)], and nutrition [e.g., carotenoids (5)]. Plants are one of the major sources of isoprenoids. However, the plant-based supply of isoprenoids suffers from low yields, impurities, and the consumption of large amounts of natural resources. Owing to the structural complexity of many isoprenoids, their chemical syntheses are inherently difficult and costly. For these reasons, the engineering of metabolic pathways for large-scale and cost-effective industrial production presents an attractive alternative source of isoprenoids. Most of the earlier work (up to 2003) on the metabolic engineering of isoprenoids was focused on carotenoids (123). Recent advances in systems biology and synthetic biology (124, 125), including high-throughput screening, low-cost gene synthesis, high-speed DNA sequencing, and protein engineering, have enabled the development of commercially viable, microbial fermentation processes for isoprenoid production. Thus far, the MVA pathway has been a superior biosynthetic route for industrial-scale isoprenoid production. The current level of MEP pathway–based terpenoid production is substantially lower than that of the engineered MVA pathway. However, pursuing MEP pathway–based isoprenoid production offers several potential advantages, including a theoretically better stoichiometric yield and lower oxygen consumption during fermentation. In this section, we summarize the lessons learned

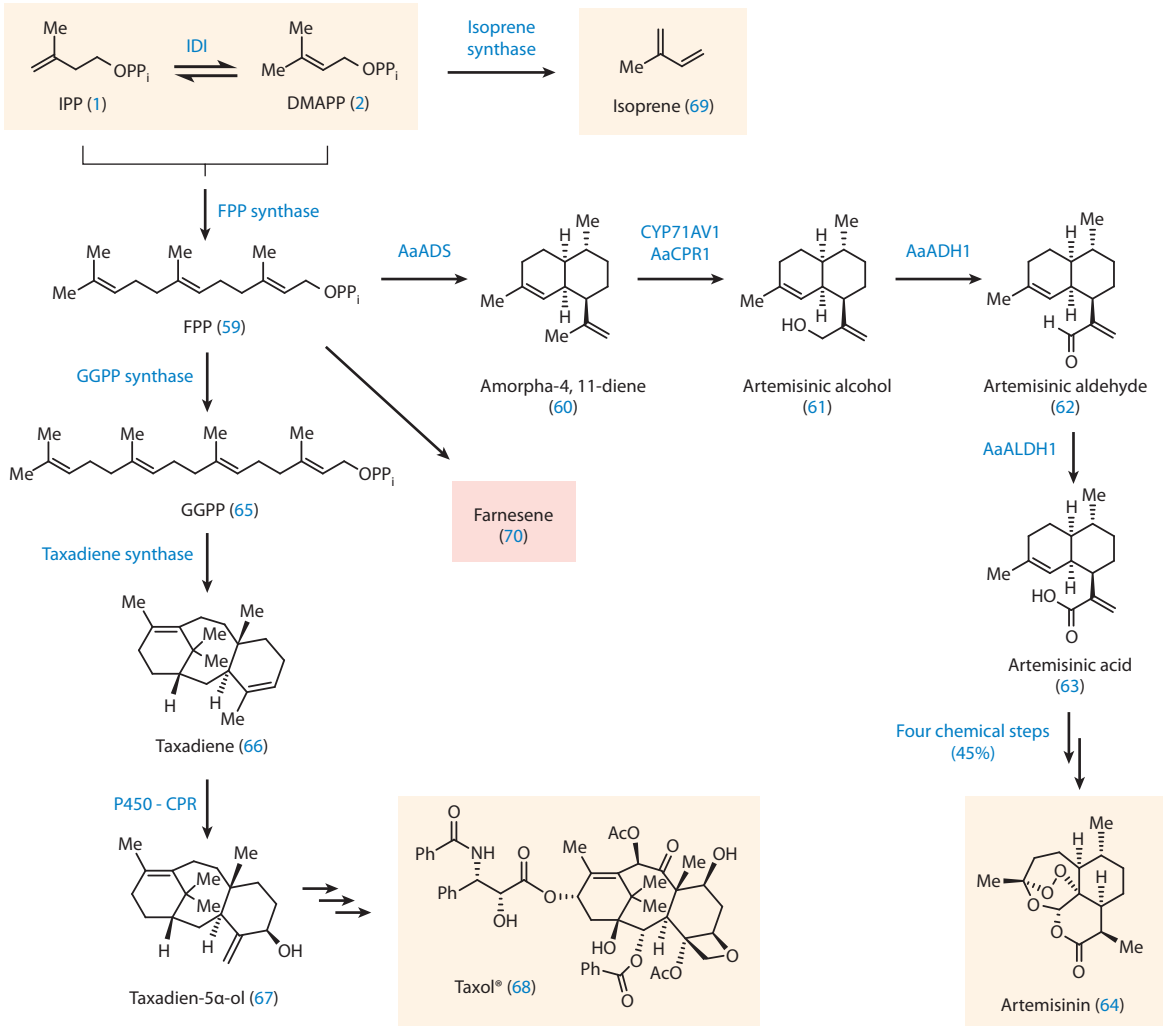

Figure 9

High-level microbial production of artemisinin precursors, isoprene, and Taxol precursors through metabolic engineering of either the mevalonic acid (MVA) or methylerythritol phosphate (MEP) pathway. Isoprenoid production through metabolic engineering normally involves two parts (using sesquiterpenes and diterpenes as examples): the production of a common intermediate FPP (farnesyl diphosphate) (**59**) by FPP synthase from IPP (isopentenyl diphosphate) (**1**) and DMAPP (dimethylallyl diphosphate) (**2**), supplied by either the MEP or the MVA pathway (**Figure 1**), and the conversion of FPP to a product of interest [e.g., artemisinin (**64**), Taxol (**68**), isoprene (**69**), or farnesene (**70**)] by introducing heterologous genes into *Escherichia coli* or yeast. Abbreviations: AaADS, *Artemisia annua* amorpha-4,11-diene synthase; AaADH1, *A. annua* alcohol dehydrogenase; AaALDH1, *A. annua* aldehyde dehydrogenase; GGPP, geranylgeranyl diphosphate; IDI, IPP:DMAPP isomerase.

regarding metabolic engineering of the MVA and MEP pathways by reviewing two landmark works that led to the high-level production of artemisinin precursors (**60** and **63**) and Taxol precursors (**66** and **67**) (**Figure 9**).

Microbial Production of Artemisinic Acid by Engineering the Mevalonic Acid Pathway

Artemisinin (**64**) (**Figure 9**), also known as Qinghaosu, is a highly effective antimalarial

drug (126) used widely with other antimalarial drugs in artemisinin-based combination therapies (ACTs) (127). The current source of artemisinin is the *Artemisia annua* plant, which is subject to supply shortages and price volatility. The potential implementation of a global subsidy for ACTs will lead to a significant increase in demand for artemisinin, further exacerbating its already constrained supply (128). Finding alternative sources of artemisinin to ensure the availability of ACTs to all patients is therefore necessary. An attractive route to artemisinin, involving the microbial production of its precursor amorpha-4,11-diene (**60**) or preferably artemisinic acid (**63**) (**Figure 9**), was envisioned early on because a chemical process can convert amorpha-4,11-diene (**60**) to artemisinin (**64**) via artemisinic acid (**63**) as an intermediate (129).

The first breakthrough in high-level amorphadiene (**60**) production occurred when the MVA pathway from *Saccharomyces cerevisiae* was transplanted into *E. coli* to increase the flux to farnesyl diphosphate (FPP; **59**) (**Figure 9**) biosynthesis (130). The eight-gene pathway was divided into two operons: the top operon (MevT) comprised the first three enzymes converting acetyl-CoA to MVA (**6**) (**Figure 1*a***), and the bottom operon (MBIS) comprised five enzymes catalyzing the formation of FPP (**59**) from MVA (**Figures 1*a*** and **9**). Production of amorphadiene (**60**) in a shake flask reached 24 mg liter^{-1} in 14 h. Subsequent studies revealed that loss of volatile amorphadiene to evaporation was significant and that the development of a two-phase partitioning bioreactor that employs dodecane overlay allowed production of 0.5 g liter^{-1} of amorpha-4,11-diene (**60**) (131). Additional improvement in amorphadiene production was achieved by detecting and eliminating bottleneck steps that were generated from imbalanced expression of genes resulting from the transfer of a large pathway into a heterologous host. Amorpha-4,11-diene synthase (AaADS for the **59** → **60** conversion) (**Figure 9**) and mevalonate kinase (MVK for the **6** → **7** conversion) (**Figure 1*a***) were identified as two rate-limiting enzymes, and optimization of their expression by increasing promoter strength and plasmid copy numbers led to a sevenfold improvement in amorphadiene production (132). Buildup of HMG-CoA (**5**) was observed in the engineered *E. coli* strain, indicating that the HMGR activity was insufficient to balance the flux (**Figure 1*a***) (133). HMG-CoA accumulation inhibited cell growth and limited the pathway flux. DNA microarray analysis and targeted metabolite profiling revealed that HMG-CoA inhibits fatty acid biosynthesis in the microbial host, leading to generalized membrane stress (134). Subsequent replacement of the *S. cerevisiae* HMGR and HMG-CoA synthase with a more active homolog from *Staphylococcus aureus* eliminated the HMG-CoA accumulation and relieved its toxicity. Coupling that with concomitant fermentation development, Lenihan et al. (135) achieved high-level production of 27 g liter^{-1} of amorpha-4,11-diene (**60**).

For MVA pathway–based isoprenoid production, the yeast *S. cerevisiae* is a preferred host over *E. coli* as it employs a native MVA pathway and therefore has none of the codon bias issues faced by expression of MVA pathway genes in *E. coli*. In addition, many tailoring enzymes in isoprenoid biosynthesis (**Figure 9**) are cytochrome P450 enzymes, and yeast is a better host for their functional expression. When only AaADS (**59** → **60** conversion) (**Figure 9**) was overexpressed under the control of the *GAL1* promoter on a high-copy plasmid in the *S. cerevisiae* S288C strain, it produced a low quantity of amorphadiene (**60**) (4.4 mg liter^{-1}) (136). Further improvement of amorphadiene (**60**) yield was achieved by either overexpressing several genes (137) or overexpressing transcription factor upc2-1 to globally upregulate the MVA pathway expression (138). Meanwhile, the ergosterol pathway, which competes for FPP, was downregulated by repression of squalene synthase (*ERG9*) gene expression. Combination of these efforts elevated the amorphadiene production to 153 mg liter^{-1} in shake flasks. Subsequent extensive metabolic engineering in conjunction with optimizing fermentation processes culminated in the

GGPP: geranylgeranyl diphosphate

production of 40 g liter^{-1} of amorphadiene (**60**) (139). These engineering efforts included (*a*) switching the host from S288C to a CEN.PK2 strain, for which physiological information and performance in fermentation are better understood (140); (*b*) overexpressing the entire MVA pathway by placing all MVA pathway genes under the control of strong GAL promoters, including integrating three copies of HMGR (136); and (*c*) deleting the *GAL1* gene to eliminate the utilization of galactose to decrease the fermentation cost (141).

High-level production of amorphadiene (**60**) by fermentation of engineered yeast represents a significant milestone. Microbial production of artemisinic acid (**63**) would constitute a superior route toward the development of an economically viable process for the production of semisynthetic artemisinin (**64**) (**Figure 9**). A cytochrome P450 monooxygenase, CYP71AV1, was isolated from *A. annua* (136, 142) and was able to catalyze all three steps (**60** → **61**, **61** → **62**, and **62** → **63**) needed to oxidize amorphadiene (**60**) to artemisinic acid (**63**). When CYP71AV1, along with its cognate reductase *A. annua* CPR1 (AaCPR1), was expressed in the engineered yeast strain that accumulated 0.5 g liter^{-1} of amorphadiene (**60**), up to 100 mg liter^{-1} of artemisinic acid (**63**) was produced (136). Expression of all *A. annua*–derived genes (*AaADS*, *CYP71AV1*, and *AaCPR1*) on a single expression plasmid allowed the production of 2.5 g liter^{-1} of artemisinic acid (**63**) in a galactose-based fermentation process (135). Although CYP71AV1, along with its cognate reductase AaCPR1, can perform all three oxidations (**60** → **61**, **61** → **62**, and **62** → **63**), the accumulation of artemisinic aldehyde (**62**) in the fermentation indicated that the conversion of **62** → **63** was not effective. Introducing an aldehyde dehydrogenase (AaALDH1) from *A. annua* into the engineered CEN.PK2 strain eliminated the accumulation of artemisinic aldehyde (**62**) and dramatically increased the production of artemisinic acid (**63**) to 7.7 g liter^{-1} (143). Additional expression of an alcohol dehydrogenase (AaADH1) from *A. annua* along with fermentation condition optimization led to titers of 25 g liter^{-1} of artemisinic acid (**63**) in a 2-liter fermenter (144).

Production of Taxol Precursors by Engineering the Methylerythritol Phosphate Pathway in *Escherichia coli*

Investigators have attempted MEP pathway engineering for carotenoid (145, 146), sesquiterpene (147, 148), and diterpenoid (149) production. The most successful endeavor was the recently reported taxadiene production (**66**) (**Figure 9**) in *E. coli* with a fed-batch fermentation titer of 1 g liter^{-1} (150). Taxadiene (**66**) is a diterpene precursor for the anticancer drug Taxol (paclitaxel; **68**) (**Figure 9**) (3). The supply of Taxol and its derivatives is constrained by the limitation in its production through plant cell culture–based semisynthetic processes. Earlier work with *E. coli* engineered for taxadiene (**66**) production by expression of DXS, IDI, GGPP (geranylgeranyl diphosphate) synthase, and taxadiene synthase had little success (titer of 1.3 mg liter^{-1}) (151). The key engineering strategy employed by Ajikumar et al. (150) was a focused combinatorial approach designed to identify an optimally balanced pathway while searching a small combinatorial space. To implement this approach, the taxadiene pathway was partitioned into modules separated at the IPP node. The first module comprised eight upstream MEP pathway genes (**Figure 1*c***), but only four (*dxs*, *idi*, *ispD*, and *ispF*) were chosen for modulation. The second module comprised two downstream synthetic genes encoding GGPP synthase and taxadiene synthase for conversion of IPP/DMAPP to taxadiene (**Figure 9**). The expression of upstream and downstream pathways was modulated by varying the promoters (Trc, T5, and T7) and gene copy numbers, resulting in drastic changes in taxadiene production levels. An unexpected but potentially important result was that a metabolic by-product, indole, showed a negative correlation with taxadiene accumulation. Although there may be a

possible synergistic effect between indole and isoprenoid pathway intermediates in inhibiting cell growth, the biochemical mechanism of indole interaction with the MEP pathway remains obscure. However, the best strain identified from the multivariate optimization appeared to have mitigated the indole's effect and could produce 1 g liter^{-1} of taxadiene (**66**) in a fed-batch fermentation. Further introduction of a chimeric fusion of taxadiene 5α-hydroxylase from *Taxus cuspidata* along with its CYP450 reductase into the taxadiene-producing strain resulted in the production of 58 mg liter^{-1} of taxadiene-5α-ol (**67**) (**Figure 9**) and an equal amount of the by-product 5(12)-oxa-3(11)-cyclotaxane (150). This level of taxadien-5α-ol is ~2,400-fold higher than previous results. The overall productivity of taxadiene-5α-ol relative to the taxadiene-producing strain, however, was significantly reduced, underscoring the challenge of obtaining efficient hydroxylation reactions in the engineered *E. coli* strain. Although this work represents significant progress in the development of a microbial production platform for Taxol, daunting tasks remain because P450-catalyzed conversion of taxadiene to taxadien-5α-ol is one of many hydroxylation steps required for the synthesis of Taxol (**68**) (**Figure 9**).

The Methylerythritol Phosphate Pathway Versus Mevalonic Acid Pathway for Metabolic Engineering

That nature employs two biosynthetic pathways for isoprenoids not only poses an interesting evolutionary question but also spurs the debate on which pathway is a better choice for use in engineering microbes for isoprenoid production. Thus far, the MVA pathway has been a superior biosynthetic route for delivering high-level isoprenoid precursors to terpene synthases for large-scale production, as evidenced by the high-level production of amorphadiene (**60**) and arteminisic acid (**63**) described above. MEP pathway–based taxadiene production in *E. coli* (150) demonstrated that the MEP pathway has the potential to support high flux. The current level of MEP pathway–based terpenoid production is substantially lower than that of the engineered MVA pathway. The limitations of the MEP pathway were initially attributed to unknown regulatory control over MEP pathway expression in *E. coli* and later to the accumulation of the metabolic indole caused by the imbalanced pathway expression, leading to inhibition of the pathway activity (150). However, the IspG and IspH enzymes may also limit the kinetic capacity of the MEP pathway because their in vitro activities are one to two orders of magnitude less than those of other MEP pathway enzymes.

To avoid the intrinsic regulation mechanism of the MEP pathway in *E. coli*, an obvious and interesting direction in MEP pathway engineering would be its transplantation to a eukaryotic host such as *S. cerevisiae*. Two major challenges exist in building a functional MEP pathway in yeast. First, the functional expression of the two iron-sulfur enzymes (IspG and IspH) is complicated, as the yeast cytosol possesses a different FeS assembly machinery relative to bacteria (152). A second challenge arises from the identification of the redox partners required for IspG and IspH activity in yeast. As discussed previously, the exact identities of in vivo redox partner proteins (and their corresponding genes) for most IspG and IspH enzymes remain largely unknown. In addition, there are no [2Fe-2S] ferredoxin or flavodoxin homologs to the known ferredoxins (plants) or flavodoxins (bacteria such as *E. coli*) in the cytosol of *S. cerevisiae* (153). An attempt to build a heterologous MEP pathway in *S. cerevisiae* has been described (154), in which the seven genes encoding the *E. coli* MEP pathway were cloned and expressed in *S. cerevisiae*, but no redox genes for either IspG or IspH were included. Unsurprisingly, the study did not generate definitive evidence that the transplanted pathway is functional in yeast. Despite these challenges, there are several potential advantages in pursuing MEP pathway–based isoprenoid production. First, the MEP pathway provides higher maximal stoichiometric yield from the feedstock

than the MVA pathway because it loses less carbon to CO_2 and is also redox balanced. The theoretical mass yield of terpenes from glucose is 30% from DXP (**12**) as compared with 25% from MVA (**6**) (155, 156). Second, the MEP pathway requires much less oxygen than the MVA pathway for the production of terpenes, which is economically beneficial to large-scale fermentations in which high rates of oxygen delivery can be both challenging and expensive.

SUMMARY POINTS

1. In the past two decades, two of the most important discoveries in isoprenoid biosynthetic studies have been the MEP pathway and a modified MVA pathway. Owing to the well-defined distribution of the MVA and MEP pathways among different kingdoms, the MEP pathway enzymes have been proposed to be ideal targets for development of new antibiotics and herbicides.
2. Investigators have reached consensus on the catalytic mechanisms of most MEP pathway enzymes (DXS, DXR, IspD, IspE, and IspF), which are summarized here.
3. For the remaining two enzymes (IspG and IspH), combined efforts from several laboratories have led to improvement of their in vitro activities by several orders of magnitude, whereas their catalytic mechanisms are still highly debated for at least two reasons: (*a*) the properties of their iron-sulfur clusters have not been fully elucidated, and (*b*) no kinetically competent intermediates have been trapped and characterized.
4. One of the trends witnessed in the past decade is the shift of focus from demonstrating the ability to make various isoprenoids to industrializing MEP or MVA pathway–based production of isoprenoids via microbial fermentations on a large scale. Knowledge and tools from several disciplines (e.g., systems biology and protein engineering) can be combined to maximize the carbon flux into the desired products.

FUTURE ISSUES

1. With structural and mechanistic information on almost all MEP pathway enzymes, one future focus is to develop mechanism-based inhibitors and demonstrate their potential as new antibiotics or herbicides.
2. Several mechanistic issues remain to be resolved for both IspG and IspH: (*a*) their in vivo reduction systems, (*b*) the functional properties of their iron-sulfur clusters, and (*c*) the trapping and characterization of kinetically competent intermediates.
3. MVA pathway–based production of isoprene at a titer of 60 g liter^{-1} has been achieved, but it is only at ~11% mass yield and less than half of the maximal yield calculated for the MVA pathway (156). Achieving maximal yield through enzyme discovery and engineering (150, 157, 158) in conjunction with optimizing microbial fermentation processes will continue to be a focus. Such efforts may allow the development of isoprenoids as renewable chemicals and transportation fuels, such as isoprene and farnesene (**69** and **70**, **Figure 9**) (155, 159–161).

4. Isoprenoid production through MEP pathway–based metabolic engineering has several advantages, as outlined earlier. Challenges remain in building a functional MEP pathway for isoprenoid production in *E. coli* or yeast, including the identification of the in vivo redox partner proteins (and their corresponding genes) for IspG and IspH, efficient incorporation of iron-sulfur clusters into the engineered strains (*E. coli* or yeast), and the elucidation and manipulation of the intrinsic regulatory mechanisms of the MEP pathway.
5. Addressing these challenges will not only offer the opportunity to develop new antimicrobial drugs by targeting the MEP pathway enzymes but also push the engineered microbes to the limit of theoretical yields to produce isoprenoids from renewable feedstocks. The success of these endeavors will help realize the enormous potential of microbes as a sustainable, environmentally friendly solution to current health, energy, and environmental problems.

DISCLOSURE STATEMENT

The authors are not aware of any affiliations, memberships, funding, or financial holdings that might be perceived as affecting the objectivity of this review.

ACKNOWLEDGMENTS

We are grateful to Professor JoAnne Stubbe, Professor Eduardus Duin, and Dr. Reid McCarty for their critical reading of this manuscript. This work and our research in related areas are supported in part by grants from the National Institutes of Health (GM093903 to P.L. and GM040541 to H.-w.L.), the Welch Foundation (F-1511 to H.w.L.), and the National Science Foundation CAREER Program (CHE-0748504 to P.L.).

LITERATURE CITED

1. Ajikumar PK, Tyo K, Carlsen S, Mucha O, Phon TH, Stephanopoulos G. 2008. Terpenoids: opportunities for biosynthesis of natural product drugs using engineered microorganisms. *Mol. Pharm.* 5:167–90
2. Liu C, Zhao Y, Wang Y. 2006. Artemisinin: current state and perspectives for biotechnological production of an antimalarial drug. *Appl. Microbiol. Biotech.* 72:11–20
3. Jennewein S, Croteau R. 2001. Taxol: biosynthesis, molecular genetics, and biotechnological applications. *Appl. Microbiol. Biotech.* 57:13–19
4. Bakkali F, Averbeck S, Averbeck D, Idaomar M. 2008. Biological effects of essential oils—a review. *Food Chem. Toxicol.* 46:446–75
5. Fraser PD, Bramley PM. 2004. The biosynthesis and nutritional uses of carotenoids. *Prog. Lipid Res.* 43:228–65
6. Bloch K. 1992. Sterol molecule: structure, biosynthesis, and function. *Steroids* 57:378–83
7. Bach TJ. 1995. Some new aspects of isoprenoid biosynthesis in plants—a review. *Lipids* 30:191–202
8. Eisenreich W, Bacher A, Arigoni D, Rohdich F. 2004. Biosynthesis of isoprenoids via the non-mevalonate pathway. *Cell. Mol. Life Sci.* 61:1401–26
9. Rohmer M. 2007. Diversity in isoprene unit biosynthesis: the methylerythritol phosphate pathway in bacteria and plastids. *Pure Appl. Chem.* 79:739–51
10. Rohmer M. 1999. The discovery of a mevalonate-independent pathway for isoprenoid biosynthesis in bacteria, algae and higher plants. *Nat. Prod. Rep.* 16:565–74
11. Hale I, O'Neill PM, Berry NG, Odom A, Sharma R. 2012. The MEP pathway and the development of inhibitors as potential anti-infective agents. *MedChemComm* 3:418–33

12. Obiol-Pardo C, Rubio-Martinez J, Imperial S. 2011. The methylerythritol phosphate (MEP) pathway for isoprenoid biosynthesis as a target for the development of new drugs against tuberculosis. *Curr. Med. Chem.* 18:1325–38
13. Wiemer AJ, Hsiao CH, Wiemer DF. 2010. Isoprenoid metabolism as a therapeutic target in gram-negative pathogens. *Curr. Top. Med. Chem.* 10:1858–71
14. Gräwert T, Groll M, Rohdich F, Bacher A, Eisenreich W. 2011. Biochemistry of the non-mevalonate isoprenoid pathway. *Cell. Mol. Life Sci.* 68:3797–814
15. Rohmer M. 2010. Methylerythritol phosphate pathway. In *Comprehensive Natural Products II—Chemistry and Biology*, ed. H-w Liu, L Mander, pp. 517–56. Oxford: Elsevier Science
16. Wiesner J, Jomaa H. 2007. Isoprenoid biosynthesis of the apicoplast as drug target. *Curr. Drug Targets* 8:3–13
17. Grochowski LL, Xu H, White RH. 2006. *Methanocaldococcus jannaschii* uses a modified mevalonate pathway for biosynthesis of isopentenyl diphosphate. *J. Bacteriol.* 188:3192–98
18. Chen M, Poulter CD. 2010. Characterization of thermophilic archaeal isopentenyl phosphate kinases. *Biochemistry* 49:207–17
19. Mabanglo MF, Schubert HL, Chen M, Hill CP, Poulter CD. 2010. X-ray structures of isopentenyl phosphate kinase. *ACS Chem. Biol.* 5:517–27
20. Dellas N, Noel JP. 2010. Mutation of archaeal isopentenyl phosphate kinase highlights mechanism and guides phosphorylation of additional isoprenoid monophosphates. *ACS Chem. Biol.* 5:589–601
21. Rohmer M, Knani M, Simonin P, Sutter B, Sahm H. 1993. Isoprenoid biosynthesis in bacteria: a novel pathway for the early steps leading to isopentenyl diphosphate. *Biochem. J.* 295(Pt. 2):517–24
22. Schwarz H. 1994. *Terpene-biosynthese in Ginkgo biloba: Eine überraschende Geschichte*. Zürich: Eidgenössische Technische Hochschule
23. Kuzuyama T, Takagi M, Takahashi S, Seto H. 2000. Cloning and characterization of 1-deoxy-D-xylulose 5-phosphate synthase from *Streptomyces* sp. strain CL190, which uses both the mevalonate and nonmevalonate pathways for isopentenyl diphosphate biosynthesis. *J. Bacteriol.* 182:891–97
24. Hahn FM, Eubanks LM, Testa CA, Blagg BSJ, Baker JA, Poulter CD. 2001. 1-Deoxy-D-xylulose 5-phosphate synthase, the gene product of open reading frame (ORF) 2816 and ORF 2895 in *Rhodobacter capsulatus*. *J. Bacteriol.* 183:1–11
25. Xiang S, Usunow G, Lange G, Busch M, Tong L. 2007. Crystal structure of 1-deoxy-D-xylulose 5-phosphate synthase, a crucial enzyme for isoprenoids biosynthesis. *J. Biol. Chem.* 282:2676–82
26. David S, Estramareix B, Fischer JC, Therisod M. 1982. The biosynthesis of thiamine. Syntheses of [1,1,1,5-$^2H_4$]-1-deoxy-D-threo-2-pentulose and incorporation of this sugar in biosynthesis of thiazole by *Escherichia coli* cells. *J. Chem. Soc.* 1982:2131–37
27. Cane DE, Du S, Robinson JK, Hsiung Y, Spenser ID. 1999. Biosynthesis of vitamin B-6: enzymatic conversion of 1-deoxy-D-xylulose-5-phosphate to pyridoxol phosphate. *J. Am. Chem. Soc.* 121:7722–23
28. Eubanks LM, Poulter CD. 2003. *Rhodobacter capsulatus* 1-deoxy-D-xylulose 5-phosphate synthase: steady-state kinetics and substrate binding. *Biochemistry* 42:1140–49
29. Hoeffler JF, Tritsch D, Grosdemange-Billiard C, Rohmer M. 2002. Isoprenoid biosynthesis via the methylerythritol phosphate pathway—mechanistic investigations of the 1-deoxy-D-xylulose 5-phosphate reductoisomerase. *Eur. J. Biochem.* 269:4446–57
30. Proteau PJ. 2004. 1-Deoxy-D-xylulose 5-phosphate reductoisomerase: an overview. *Bioorg. Chem.* 32:483–93
31. Argyrou A, Blanchard JS. 2004. Kinetic and chemical mechanism of *Mycobacterium tuberculosis* 1-deoxy-D-xylulose-5-phosphate isomeroreductase. *Biochemistry* 43:4375–84
32. Fox DT, Poulter CD. 2005. Mechanistic studies with 2-*C*-methyl-D-erythritol 4-phosphate synthase from *Escherichia coli*. *Biochemistry* 44:8360–68
33. Wong U, Cox RJ. 2007. The chemical mechanism of D-1-deoxyxylulose-5-phosphate reductoisomerase from *Escherichia coli*. *Angew. Chem. Int. Ed.* 46:4926–29
34. Munos JW, Pu X, Mansoorabadi SO, Kim HJ, Liu H-w. 2009. A secondary kinetic isotope effect study of the 1-deoxy-D-xylulose-5-phosphate reductoisomerase-catalyzed reaction: evidence for a retroaldol-aldol rearrangement. *J. Am. Chem. Soc.* 131:2048–49

35. Mac Sweeney A, Lange R, Fernandes RP, Schulz H, Dale GE, et al. 2005. The crystal structure of *E.coli* 1-deoxy-D-xylulose-5-phosphate reductoisomerase in a ternary complex with the antimalarial compound fosmidomycin and NADPH reveals a tight-binding closed enzyme conformation. *J. Mol. Biol.* 345:115–27
36. Lauw S, Illarionova V, Bacher A, Rohdich F, Eisenreich W. 2008. Biosynthesis of isoprenoids: studies on the mechanism of 2*C*-methyl-D-erythritol-4-phosphate synthase. *FEBS J.* 275:4060–73
37. Fox DT, Poulter CD. 2005. Synthesis and evaluation of 1-deoxy-D-xylulose 5-phosphoric acid analogues as alternate substrates for methylerythritol phosphate synthase. *J. Org. Chem.* 70:1978–85
38. Meyer O, Grosdemange-Billiard C, Tritsch D, Rohmer M. 2007. Synthesis and activity of two trifluorinated analogues of 1-deoxy-D-xylulose 5-phosphate. *Tetrahedron Lett.* 48:711–14
39. Fernandes RPM, Phaosiri C, Proteau PJ. 2005. Mutation in the flexible loop of 1-deoxy-D-xylulose 5-phosphate reductoisomerase broadens substrate utilization. *Arch. Biochem. Biophys.* 444:159–64
40. Munos JW, Pu X, Liu H-w. 2008. Synthesis and analysis of a fluorinated product analogue as an inhibitor for 1-deoxy-D-xylulose 5-phosphate reductoisomerase. *Bioorg. Med. Chem. Lett.* 18:3090–94
41. Herz S, Wungsintaweekul J, Schuhr CA, Hecht S, Luttgen H, et al. 2000. Biosynthesis of terpenoids: YgbB protein converts 4-diphosphocytidyl-2C-methyl-D-erythritol 2-phosphate to 2C-methyl-D-erythritol 2,4-cyclodiphosphate. *Proc. Natl. Acad. Sci. USA* 97:2486–90
42. Rohdich F, Eisenreich W, Wungsintaweekul J, Hecht S, Schuhr CA, Bacher A. 2001. Biosynthesis of terpenoids. 2*C*-Methyl-D-erythritol 2,4-cyclodiphosphate synthase (IspF) from *Plasmodium falciparum*. *Eur. J. Biochem.* 268:3190–97
43. Testa CA, Lherbet C, Pojer F, Noel JP, Poulter CD. 2006. Cloning and expression of *IspDF* from *Mesorhizobium loti*. Characterization of a bifunctional protein that catalyzes non-consecutive steps in the methylerythritol phosphate pathway. *Biochim. Biophys. Acta* 1764:85–96
44. Gabrielsen M, Rohdich F, Eisenreich W, Gräwert T, Hecht S, et al. 2004. Biosynthesis of isoprenoids: a bifunctional IspDF enzyme from *Campylobacter jejuni*. *Eur. J. Biochem.* 271:3028–35
45. Gabrielsen M, Bond CS, Hallyburton I, Hecht S, Bacher A, et al. 2004. Hexameric assembly of the bifunctional methylerythritol 2,4-cyclodiphosphate synthase and protein-protein associations in the deoxyxylulose-dependent pathway of isoprenoid precursor biosynthesis. *J. Biol. Chem.* 279:52753–61
46. Baker J, Franklin DB, Parker J. 1992. Sequence and characterization of the *gcpE* gene of *Escherichia coli*. *FEMS Microbiol. Lett.* 73:175–80
47. Campos N, Rodríguez-Concepción M, Seemann M, Rohmer M, Boronat A. 2001. Identification of *gcpE* as a novel gene of the 2-*C*-methyl-D-erythritol 4-phosphate pathway for isoprenoid biosynthesis in *Escherichia coli*. *FEBS Lett.* 488:170–3
48. Altincicek B, Kollas AK, Sanderbrand S, Wiesner J, Hintz M, et al. 2001. GcpE is involved in the 2-*C*-methyl-D-erythritol 4-phosphate pathway of isoprenoid biosynthesis in *Escherichia coli*. *J. Bacteriol.* 183:2411–16
49. Hecht S, Eisenreich W, Adam P, Amslinger S, Kis K, et al. 2001. Studies on the nonmevalonate pathway to terpenes: the role of the GcpE (IspG) protein. *Proc. Natl. Acad. Sci. USA* 98:14837–42
50. Seemann M, Campos N, Rodríguez-Concepción M, Ibañez E, Duvold T, et al. 2002. Isoprenoid biosynthesis in *Escherichia coli* via the methylerythritol phosphate pathway: enzymatic conversion of methylerythritol cyclodiphosphate into a phosphorylated derivative of (*E*)-2-methylbut-2-ene-1,4-diol. *Tetrahedron Lett.* 43:1413–15
51. Seemann M, Campos N, Rodríguez-Concepción M, Hoeffler J-F, Grosdemange-Billiard C, et al. 2002. Isoprenoid biosynthesis via the methylerythritol phosphate pathway: accumulation of 2-*C*-methyl-D-erythritol 2,4-cyclodiphosphate in a *gcpE* deficient mutant of *Escherichia coli*. *Tetrahedron Lett.* 43:775–78
52. Zepeck F, Gräwert T, Kaiser J, Schramek N, Eisenreich W, et al. 2005. Biosynthesis of isoprenoids. Purification and properties of IspG protein from *Escherichia coli*. *J. Org. Chem.* 70:9168–74
53. Xiao Y, Zahariou G, Sanakis Y, Liu P. 2009. IspG enzyme activity in the deoxyxylulose phosphate pathway: roles of the iron-sulfur cluster. *Biochemistry* 48:10483–85
54. Johnson DC, Dean DR, Smith AD, Johnson MK. 2005. Structure, function, and formation of biological iron-sulfur clusters. *Annu. Rev. Biochem.* 74:247–81

55. Loiseau L, Gerez C, Bekker M, Ollagnier-de Choudens S, Py B, et al. 2007. ErpA, an iron-sulfur (Fe-S) protein of the A-type essential for respiratory metabolism in *Escherichia coli*. *Proc. Natl. Acad. Sci. USA* 104:13626–31
56. Kollas AK, Duin EC, Eberl M, Altincicek B, Hintz M, et al. 2002. Functional characterization of GcpE, an essential enzyme of the non-mevalonate pathway of isoprenoid biosynthesis. *FEBS Lett.* 532:432–36
57. Seemann M, Wegner P, Schunemann V, Bui BT, Wolff M, et al. 2005. Isoprenoid biosynthesis in chloroplasts via the methylerythritol phosphate pathway: the (*E*)-4-hydroxy-3-methylbut-2-enyl diphosphate synthase (GcpE) from *Arabidopsis thaliana* is a [4Fe-4S] protein. *J. Biol. Inorg. Chem.* 10:131–37
58. Lee M, Gräwert T, Quitterer F, Rohdich F, Eppinger J, et al. 2010. Biosynthesis of isoprenoids: crystal structure of the [4Fe-4S] cluster protein IspG. *J. Mol. Biol.* 404:600–10
59. Rekittke I, Nonaka T, Wiesner J, Demmer U, Warkentin E, et al. 2011. Structure of the E-1-hydroxy-2-methyl-but-2-enyl-4-diphosphate synthase (GcpE) from *Thermus thermophilus*. *FEBS Lett.* 585:447–51
60. Rees DC, Howard JB. 2003. The interface between the biological and inorganic worlds: iron-sulfur metalloclusters. *Science* 300:929–31
61. Beinert H, Holm RH, Munck E. 1997. Iron-sulfur clusters: nature's modular, multipurpose structures. *Science* 277:653–59
62. Puan KJ, Wang H, Dairi T, Kuzuyama T, Morita CT. 2005. *fldA* is an essential gene required in the 2-C-methyl-D-erythritol 4-phosphate pathway for isoprenoid biosynthesis. *FEBS Lett.* 579:3802–6
63. Seemann M, Tse Sum Bui B, Wolff M, Miginiac-Maslow M, Rohmer M. 2006. Isoprenoid biosynthesis in plant chloroplasts via the MEP pathway: direct thylakoid/ferredoxin-dependent photoreduction of GcpE/IspG. *FEBS Lett.* 580:1547–52
64. Okada K, Hase T. 2005. Cyanobacterial non-mevalonate pathway: (*E*)-4-hydroxy-3-methylbut-2-enyl diphosphate synthase interacts with ferredoxin in *Thermosynechococcus elongatus* BP-1. *J. Biol. Chem.* 280:20672–79
65. Xu W, Lees NS, Adedeji D, Wiesner J, Jomaa H, et al. 2010. Paramagnetic intermediates of (*E*)-4-hydroxy-3-methylbut-2-enyl diphosphate synthase (GcpE/IspG) under steady-state and pre-steady-state conditions. *J. Am. Chem. Soc.* 132:14509–20
66. Adedeji D, Hernandez H, Wiesner J, Köhler U, Jomaa H, Duin EC. 2007. Possible direct involvement of the active-site [4Fe-4S] cluster of the GcpE enzyme from *Thermus thermophilus* in the conversion of MEcPP. *FEBS Lett.* 581:279–83
67. Rohdich F, Zepeck F, Adam P, Hecht S, Kaiser J, et al. 2003. The deoxyxylulose phosphate pathway of isoprenoid biosynthesis: studies on the mechanisms of the reactions catalyzed by IspG and IspH protein. *Proc. Natl. Acad. Sci. USA* 100:1586–91
68. Itoh T, Nagano T, Sato M, Hirobe M. 1989. Deoxygenation of oxiran compounds to olefins by $[Fe_4S_4(Sc_6H_5)_4]^{2-}$ in the presence of $NaBH_4$. *Tetrahedron Lett.* 30:6387–88
69. Seemann M, Bui BTS, Wolff M, Tritsch D, Campos N, et al. 2002. Isoprenoid biosynthesis through the methylerythritol phosphate pathway: The (*E*)-4-hydroxy-3-methylbut-2-enyl diphosphate synthase (GcpE) is a [4Fe-4S] protein. *Angew. Chem. Int. Ed.* 41:4337–39
70. Xiao Y, Rooker D, You Q, Meyers CLF, Liu P. 2011. IspG-catalyzed positional isotopic exchange in methylerythritol cyclodiphosphate of the deoxyxylulose phosphate pathway: mechanistic implications. *ChemBiochem* 12:527–30
71. Buckel W, Martins BM, Messerschmidt A, Golding BT. 2005. Radical-mediated dehydration reactions in anaerobic bacteria. *Biol. Chem.* 386:951–59
72. Beinert H, Kennedy MC, Stout CD. 1996. Aconitase as iron-sulfur protein, enzyme, and iron-regulatory protein. *Chem. Rev.* 96:2335–73
73. Wang W, Li J, Wang K, Huang C, Zhang Y, Oldfield E. 2010. Organometallic mechanism of action and inhibition of the 4Fe-4S isoprenoid biosynthesis protein GcpE (IspG). *Proc. Natl. Acad. Sci. USA* 107:11189–93
74. Wang W, Wang K, Li J, Nellutla S, Smirnova TI, Oldfield E. 2011. An ENDOR and HYSCORE investigation of a reaction intermediate in IspG (GcpE) catalysis. *J. Am. Chem. Soc.* 133:8400–3
75. Nyland RL II, Xiao Y, Liu P, Freel Meyers CL. 2009. IspG converts an epoxide substrate analogue to (*E*)-4-hydroxy-3-methylbut-2-enyl diphosphate: implications for IspG catalysis in isoprenoid biosynthesis. *J. Am. Chem. Soc.* 131:17734–35

76. Xiao Y, Nyland RL II, Meyers CL, Liu P. 2010. Methylerythritol cyclodiphosphate (MEcPP) in deoxyxylulose phosphate pathway: synthesis from an epoxide and mechanisms. *Chem. Commun.* 46:7220–22
77. Brandt W, Dessoy MA, Fulhorst M, Gao W, Zenk MH, Wessjohann LA. 2004. A proposed mechanism for the reductive ring opening of the cyclodiphosphate MEcPP, a crucial transformation in the new DXP/MEP pathway to isoprenoids based on modeling studies and feeding experiments. *ChemBiochem* 5:311–23
78. Wolff M, Seemann M, Tse Sum Bui B, Frapart Y, Tritsch D, et al. 2003. Isoprenoid biosynthesis via the methylerythritol phosphate pathway: the (*E*)-4-hydroxy-3-methylbut-2-enyl diphosphate reductase (LytB/IspH) from *Escherichia coli* is a [4Fe-4S] protein. *FEBS Lett.* 541:115–20
79. Rohdich F, Hecht S, Gärtner K, Adam P, Krieger C, et al. 2002. Studies on the nonmevalonate terpene biosynthetic pathway: metabolic role of IspH (LytB) protein. *Proc. Natl. Acad. Sci. USA* 99:1158–63
80. Street IP, Christensen DJ, Poulter CD. 1990. Hydrogen exchange during the enzyme-catalyzed isomerization of isopentenyl diphosphate and dimethylallyl diphosphate. *J. Am. Chem. Soc.* 112:8577–78
81. Adam P, Hecht S, Eisenreich WG, Kaiser J, Gräwert T, et al. 2002. Biosynthesis of terpenes: studies on 1-hydroxy-2-methyl-2-(*E*)-butenyl 4-diphosphate reductase. *Proc. Natl. Acad. Sci. USA* 99:12108–13
82. Gräwert T, Kaiser J, Zepeck F, Laupitz R, Hecht S, et al. 2004. IspH protein of *Escherichia coli:* studies on iron-sulfur cluster implementation and catalysis. *J. Am. Chem. Soc.* 126:12847–55
83. Gräwert T, Span I, Eisenreich W, Rohdich F, Eppinger J, et al. 2010. Probing the reaction mechanism of IspH protein by x-ray structure analysis. *Proc. Natl. Acad. Sci. USA* 107:1077–81
84. Altincicek B, Duin EC, Reichenberg A, Hedderich R, Kollas AK, et al. 2002. LytB protein catalyzes the terminal step of the 2-*C*-methyl-D-erythritol-4-phosphate pathway of isoprenoid biosynthesis. *FEBS Lett.* 532:437–40
85. Xiao Y, Chu L, Sanakis Y, Liu P. 2009. Revisiting the IspH catalytic system in the deoxyxylulose phosphate pathway: achieving high activity. *J. Am. Chem. Soc.* 131:9931–33
86. Seemann M, Janthawornpong K, Schweizer J, Böttger LH, Janoschka A, et al. 2009. Isoprenoid biosynthesis via the MEP pathway: In vivo Mössbauer spectroscopy identifies a $[4Fe\text{-}4S]^{2+}$ center with unusual coordination sphere in the LytB protein. *J. Am. Chem. Soc.* 131:13184–85
87. Ahrens-Botzong A, Janthawornpong K, Wolny JA, Tambou EN, Rohmer M, et al. 2011. Biosynthesis of isoprene units: Mössbauer spectroscopy of substrate and inhibitor binding to the [4Fe-4S] cluster of the LytB/IspH enzyme. *Angew. Chem. Int. Ed.* 50:11976–79
88. Rekittke I, Wiesner J, Röhrich R, Demmer U, Warkentin E, et al. 2008. Structure of (*E*)-4-hydroxy-3-methyl-but-2-enyl diphosphate reductase, the terminal enzyme of the non-mevalonate pathway. *J. Am. Chem. Soc.* 130:17206–7
89. Gräwert T, Rohdich F, Span I, Bacher A, Eisenreich W, et al. 2009. Structure of active IspH enzyme from *Escherichia coli* provides mechanistic insights into substrate reduction. *Angew. Chem. Int. Ed.* 48:5756–59
90. Bolm C, Legros J, Le Paih J, Zani L. 2004. Iron-catalyzed reactions in organic synthesis. *Chem. Rev.* 104:6217–54
91. Span I, Grawert T, Bacher A, Eisenreich W, Groll M. 2012. Crystal structures of mutant IspH proteins reveal a rotation of the substrate's hydroxymethyl group during catalysis. *J. Mol. Biol.* 416:1–9
92. Wang WX, Wang K, Liu YL, No JH, Li JK, et al. 2010. Bioorganometallic mechanism of action, and inhibition, of IspH. *Proc. Natl. Acad. Sci. USA* 107:4522–27
93. Wang W, Wang K, Span I, Jauch J, Bacher A, et al. 2012. Are free radicals involved in IspH catalysis? An EPR and crystallographic investigation. *J. Am. Chem. Soc.* 134:11225–34
94. Xiao Y, Liu P. 2008. IspH protein of the deoxyxylulose phosphate pathway: mechanistic studies with C_1-deuterium-labeled substrate and fluorinated analogue. *Angew. Chem. Int. Ed.* 47:9722–25
95. Xiao Y, Zhao ZK, Liu P. 2008. Mechanistic studies of IspH in the deoxyxylulose phosphate pathway: heterolytic C-O bond cleavage at C_4 position. *J. Am. Chem. Soc.* 130:2164–65
96. Gräwert T, Span I, Bacher A, Groll M. 2010. Reductive dehydroxylation of allyl alcohols by IspH protein. *Angew. Chem. Int. Ed.* 49:8802–9
97. Xu W, Lees NS, Hall D, Welideniya D, Hoffman BM, Duin EC. 2012. A closer look at the spectroscopic properties of possible reaction intermediates in wild-type and mutant (*E*)-4-hydroxy-3-methylbut-2-enyl diphosphate reductase. *Biochemistry* 51:4845–49

98. Chang W-c, Xiao Y, Liu H-w, Liu P. 2011. Mechanistic studies of an IspH-catalyzed reaction: implications for substrate binding and protonation in the biosynthesis of isoprenoids. *Angew. Chem. Int. Ed.* 50:12304–7
99. Janthawornpong K, Krasutsky S, Chaignon P, Rohmer M, Poulter CD, Seemann M. 2013. Inhibition of IspH, a $[4Fe–4S]^{2+}$ enzyme involved in the biosynthesis of isoprenoids via the methylerythritol phosphate pathway. *J. Am. Chem. Soc.* 135:1816–22
99a. Xiao Y, Chang WC, Liu HW, Liu P. 2011. Study of IspH, a key enzyme in the methylerythritol phosphate pathway using fluoro-substituted substrate analogues. *Org. Lett.* 13:5912–15
100. Span I, Wang K, Wang W, Jauch J, Eisenreich W, et al. 2013. Structures of fluoro, amino, and thiol inhibitors bound to the $[Fe_4S_4]$ protein IspH. *Angew. Chem. Int. Ed.* 52:2118–21
101. Laupitz R, Gräwert T, Rieder C, Zepeck F, Bacher A, et al. 2004. Stereochemical studies on the making and unmaking of isopentenyl diphosphate in different biological systems. *Chem. Biodivers.* 1:1367–76
102. Citron CA, Brock NL, Rabe P, Dickschat JS. 2012. The stereochemical course and mechanism of the IspH reaction. *Angew. Chem. Int. Ed.* 51:4053–57
103. Arigoni D, Eisenreich W, Latzel C, Sagner S, Radykewicz T, et al. 1999. Dimethylallyl pyrophosphate is not the committed precursor of isopentenyl pyrophosphate during terpenoid biosynthesis from 1-deoxyxylulose in higher plants. *Proc. Natl. Acad. Sci. USA* 96:1309–14
104. Rieder C, Jaun B, Arigoni D. 2000. On the early steps of cineol biosynthesis in *Eucalyptus globulus*. *Helv. Chim. Acta* 83:2504–13
105. Tritsch D, Hemmerlin A, Bach TJ, Rohmer M. 2010. Plant isoprenoid biosynthesis via the MEP pathway: in vivo IPP/DMAPP ratio produced by (*E*)-4-hydroxy-3-methylbut-2-enyl diphosphate reductase in tobacco BY-2 cell cultures. *FEBS Lett.* 584:129–34
106. Agranoff BW, Eggerer H, Henning U, Lynen F. 1959. Isopentenyl pyrophosphate isomerase. *J. Am. Chem. Soc.* 81:1254–55
107. Agranoff BW, Eggerer H, Henning U, Lynen F. 1960. Biosynthesis of terpenes. VII. Isopentenyl pyrophosphate isomerase. *J. Biol. Chem.* 235:326–32
108. Kaneda K, Kuzuyama T, Takagi M, Hayakawa Y, Seto H. 2001. An unusual isopentenyl diphosphate isomerase found in the mevalonate pathway gene cluster from *Streptomyces* sp. strain CL190. *Proc. Natl. Acad. Sci. USA* 98:932–37
109. Hemmi H, Ikeda Y, Yamashita S, Nakayama T, Nishino T. 2004. Catalytic mechanism of type 2 isopentenyl diphosphate:dimethylallyl diphosphate isomerase: verification of a redox role of the flavin cofactor in a reaction with no net redox change. *Biochem. Biophys. Res. Commun.* 322:905–10
110. Kittleman W, Thibodeaux CJ, Liu YN, Zhang H, Liu H-w. 2007. Characterization and mechanistic studies of type II isopentenyl diphosphate:dimethylallyl diphosphate isomerase from *Staphylococcus aureus*. *Biochemistry* 46:8401–13
111. Rothman SC, Helm TR, Poulter CD. 2007. Kinetic and spectroscopic characterization of type II isopentenyl diphosphate isomerase from *Thermus thermophilus*: evidence for formation of substrate-induced flavin species. *Biochemistry* 46:5437–45
112. Thibodeaux CJ, Mansoorabadi SO, Kittleman W, Chang W-c, Liu H-w. 2008. Evidence for the involvement of acid/base chemistry in the reaction catalyzed by the type II isopentenyl diphosphate/dimethylallyl diphosphate isomerase from *Staphylococcus aureus*. *Biochemistry* 47:2547–58
113. Johnston JB, Walker JR, Rothman SC, Poulter CD. 2007. Type-2 isopentenyl diphosphate isomerase. Mechanistic studies with cyclopropyl and epoxy analogues. *J. Am. Chem. Soc.* 129:7740–41
114. Rothman SC, Johnston JB, Lee S, Walker JR, Poulter CD. 2008. Type II isopentenyl diphosphate isomerase: irreversible inactivation by covalent modification of flavin. *J. Am. Chem. Soc.* 130:4906–13
115. Unno H, Yamashita S, Ikeda Y, Sekiguchi S, Yoshida N, et al. 2009. New role of flavin as a general acid-base catalyst with no redox function in Type 2 isopentenyl-diphosphate isomerase. *J. Biol. Chem.* 284:9160–67
116. Kao CL, Kittleman W, Zhang H, Seto H, Liu H-w. 2005. Stereochemical analysis of isopentenyl diphosphate isomerase type II from *Staphylococcus aureus* using chemically synthesized (*S*)- and (*R*)-[2-^{2}H]isopentenyl diphosphates. *Org. Lett.* 7:5677–80

117. Thibodeaux CJ, Chang W-c, Liu H-w. 2010. Linear free energy relationships demonstrate a catalytic role for the flavin mononucleotide coenzyme of the type II isopentenyl diphosphate:dimethylallyl diphosphate isomerase. *J. Am. Chem. Soc.* 132:9994–96
118. Walker JR, Rothman SC, Poulter CD. 2008. Synthesis and evaluation of substrate analogues as mechanism-based inhibitors of type II isopentenyl diphosphate isomerase. *J. Org. Chem.* 73:726–29
119. Nagai T, Unno H, Janczak MW, Yoshimura T, Poulter CD, Hemmi H. 2011. Covalent modification of reduced flavin mononucleotide in type-2 isopentenyl diphosphate isomerase by active-site-directed inhibitors. *Proc. Natl. Acad. Sci. USA* 108:20461–66
120. Hoshino T, Tamegai H, Kakinuma K, Eguchi T. 2006. Inhibition of type 2 isopentenyl diphosphate isomerase from *Methanocaldococcus jannaschii* by a mechanism-based inhibitor of type 1 isopentenyl diphosphate isomerase. *Bioorg. Med. Chem.* 14:6555–59
121. Calveras J, Thibodeaux CJ, Mansoorabadi SO, Liu H-w. 2012. Stereochemical studies of the type II isopentenyl diphosphate-dimethylallyl diphosphate isomerase implicate the FMN coenzyme in substrate protonation. *ChemBiochem* 13:42–46
122. Breitmaier E. 2006. *Terpenes: Flavors, Fragrances, Pharmaca, Pheromones*. Weinheim, Ger.: WILEY-VCH 223 pp.
123. Barkovich R, Liao JC. 2001. Metabolic engineering of isoprenoids. *Metab. Eng.* 3:27–39
124. Fu P, Panke S. 2009. *Systems Biology and Synthetic Biology*. Weinheim, Ger.: WILEY-VCH
125. Tyo KE, Alper HS, Stephanopoulos GN. 2007. Expanding the metabolic engineering toolbox: more options to engineer cells. *Trends Biotechnol.* 25:132–37
126. White NJ. 2008. Qinghaosu (artemisinin): the price of success. *Science* 320:330–34
127. World Health Organ. 2006. Guidelines for the Treatment of Malaria. Geneva: World Health Organ. 253 pp.
128. Van Noorden R. 2010. Demand for malaria drug soars. *Nature* 466:672–73
129. Hale V, Keasling JD, Renninger N, Diagana TT. 2007. Microbially derived artemisinin: a biotechnology solution to the global problem of access to affordable antimalarial drugs. *Am. J. Trop. Med. Hyg.* 77:198–202
130. Martin VJ, Pitera DJ, Withers ST, Newman JD, Keasling JD. 2003. Engineering a mevalonate pathway in *Escherichia coli* for production of terpenoids. *Nat. Biotechnol.* 21:796–802
131. Newman JD, Marshall J, Chang M, Nowroozi F, Paradise E, et al. 2006. High-level production of amorpha-4,11-diene in a two-phase partitioning bioreactor of metabolically engineered *Escherichia coli*. *Biotechnol. Bioeng.* 95:684–91
132. Anthony JR, Anthony LC, Nowroozi F, Kwon G, Newman JD, Keasling JD. 2009. Optimization of the mevalonate-based isoprenoid biosynthetic pathway in *Escherichia coli* for production of the anti-malarial drug precursor amorpha-4,11-diene. *Metab. Eng.* 11:13–19
133. Pitera DJ, Paddon CJ, Newman JD, Keasling JD. 2007. Balancing a heterologous mevalonate pathway for improved isoprenoid production in *Escherichia coli*. *Metab. Eng.* 9:193–207
134. Kizer L, Pitera DJ, Pfleger BF, Keasling JD. 2008. Application of functional genomics to pathway optimization for increased isoprenoid production. *Appl. Environ. Microbiol.* 74:3229–41
135. Lenihan JR, Tsuruta H, Diola D, Renninger NS, Regentin R. 2008. Developing an industrial artemisinic acid fermentation process to support the cost-effective production of antimalarial artemisinin-based combination therapies. *Biotechnol. Prog.* 24:1026–32
136. Ro DK, Paradise EM, Ouellet M, Fisher KJ, Newman KL, et al. 2006. Production of the antimalarial drug precursor artemisinic acid in engineered yeast. *Nature* 440:940–43
137. Donald KA, Hampton RY, Fritz IB. 1997. Effects of overproduction of the catalytic domain of 3-hydroxy-3-methylglutaryl coenzyme A reductase on squalene synthesis in *Saccharomyces cerevisiae*. *Appl. Environ. Microbiol.* 63:3341–44
138. Davies BS, Wang HS, Rine J. 2005. Dual activators of the sterol biosynthetic pathway of *Saccharomyces cerevisiae*: similar activation/regulatory domains but different response mechanisms. *Mol. Cell. Biol.* 25:7375–85
139. Westfall PJ, Pitera DJ, Lenihan JR, Eng D, Woolard F, et al. 2012. Production of amorphadiene in yeast, and its conversion to dihydroartemisinic acid, precursor to the antimalarial agent artemisinin. *Proc. Natl. Acad. Sci. USA* 109:E111–18

140. van Dijken JP, Bauer J, Brambilla L, Duboc P, Francois JM, et al. 2000. An interlaboratory comparison of physiological and genetic properties of four *Saccharomyces cerevisiae* strains. *Enzyme Microb. Technol.* 26:706–14
141. Hovland P, Flick J, Johnston M, Sclafani RA. 1989. Galactose as a gratuitous inducer of *GAL* gene expression in yeasts growing on glucose. *Gene* 83:57–64
142. Teoh KH, Polichuk DR, Reed DW, Nowak G, Covello PS. 2006. *Artemisia annua* L. (Asteraceae) trichome-specific cDNAs reveal CYP71AV1, a cytochrome P450 with a key role in the biosynthesis of the antimalarial sesquiterpene lactone artemisinin. *FEBS Lett.* 580:1411–16
143. Teoh KH, Polichuk DR, Reed DW, Covello PS. 2009. Molecular cloning of an aldehyde dehydrogenase implicated in artemisinin biosynthesis in *Artemisia annua*. *Botany* 87:635–42
144. Tsuruta H, Paddon CJ, Eng D, Lenihan JR, Horning T, et al. 2009. High-level production of amorpha-4,11-diene, a precursor of the antimalarial agent artemisinin, in *Escherichia coli*. *PLoS ONE* 4:e4489
145. Farmer WR, Liao JC. 2001. Precursor balancing for metabolic engineering of lycopene production in *Escherichia coli*. *Biotechnol. Prog.* 17:57–61
146. Kim SW, Keasling JD. 2001. Metabolic engineering of the nonmevalonate isopentenyl diphosphate synthesis pathway in *Escherichia coli* enhances lycopene production. *Biotechnol. Bioeng.* 72:408–15
147. Martin VJ, Yoshikuni Y, Keasling JD. 2001. The in vivo synthesis of plant sesquiterpenes by *Escherichia coli*. *Biotechnol. Bioeng.* 75:497–503
148. Cane DE, Wu Z, Oliver JS, Hohn TM. 1993. Overproduction of soluble trichodiene synthase from *Fusarium sporotrichioides* in *Escherichia coli*. *Arch. Biochem. Biophys.* 300:416–22
149. Morrone D, Lowry L, Determan MK, Hershey DM, Xu M, Peters RJ. 2010. Increasing diterpene yield with a modular metabolic engineering system in *E. coli*: comparison of MEV and MEP isoprenoid precursor pathway engineering. *Appl. Microbiol. Biotechnol.* 85:1893–906
150. Ajikumar PK, Xiao WH, Tyo KE, Wang Y, Simeon F, et al. 2010. Isoprenoid pathway optimization for Taxol precursor overproduction in *Escherichia coli*. *Science* 330:70–74
151. Huang Q, Roessner CA, Croteau R, Scott AI. 2001. Engineering *Escherichia coli* for the synthesis of taxadiene, a key intermediate in the biosynthesis of taxol. *Bioorg. Med. Chem.* 9:2237–42
152. Lill R, Muhlenhoff U. 2008. Maturation of iron-sulfur proteins in eukaryotes: mechanisms, connected processes, and diseases. *Annu. Rev. Biochem.* 77:669–700
153. Liger D, Graille M, Zhou CZ, Leulliot N, Quevillon-Cheruel S, et al. 2004. Crystal structure and functional characterization of yeast YLR011wp, an enzyme with NAD(P)H-FMN and ferric iron reductase activities. *J. Biol. Chem.* 279:34890–97
154. Maury J, Asadollahi MA, Moller K, Schalk M, Clark A, et al. 2008. Reconstruction of a bacterial isoprenoid biosynthetic pathway in *Saccharomyces cerevisiae*. *FEBS Lett.* 582:4032–38
155. Rude MA, Schirmer A. 2009. New microbial fuels: a biotech perspective. *Curr. Opin. Microbiol.* 12:274–81
156. Whited GM, Feher FJ, Benko DA, Cervin MA, Chotani GK, et al. 2010. Technology update: development of a gas-phase bioprocess for isoprene-monomer production using metabolic pathway engineering. *Ind. Biotechnol.* 6:152–63
157. Cane DE. 1990. Enzymatic formation of sesquiterpenes. *Chem. Rev.* 90:1089–103
158. Chang MC, Eachus RA, Trieu W, Ro DK, Keasling JD. 2007. Engineering *Escherichia coli* for production of functionalized terpenoids using plant P450s. *Nat. Chem. Biol.* 3:274–77
159. Zhang F, Rodriguez S, Keasling JD. 2011. Metabolic engineering of microbial pathways for advanced biofuels production. *Curr. Opin. Biotechnol.* 22:1–9
160. Renninger NS, McPhee DJ. 2008. Fuel compositions comprising farnesane and farnesane derivatives and method of making and using same. *U.S. Patent No. 2,008,045,555*
161. Tsuruta H, Lenihan JR, Regentin R. 2009. Production of isoprenoids. *U.S. Patent No. WO2009042070A2*

Annual Review of Biochemistry
Volume 82, 2013

Contents

Prefatory

Recent Advances in Biochemistry

Indexes

Errata

An online log of corrections to *Annual Review of Biochemistry* articles may be found at http://biochem.annualreviews.org/errata.shtml